

LEARNING PARAMETRIC KOOPMAN DECOMPOSITIONS FOR PREDICTION AND CONTROL*

YUE GUO[†], MILAN KORDA[‡], IOANNIS G. KEVREKIDIS[§], AND QIANXIAO LI[¶]

Abstract. We present an approach to constructing approximate Koopman-type decompositions for dynamical systems depending on static or time-varying parameters. Our method simultaneously constructs an invariant subspace *and* a parametric family of projected Koopman operators acting on this subspace. We parametrize *both the projected Koopman operator family and the dictionary that spans the invariant subspace* by neural networks, and jointly train them with trajectory data. We show theoretically the validity of our approach, and demonstrate via numerical experiments that it exhibits significant improvements over existing methods in solving prediction problems, especially those with large state or parameter dimensions, and those possessing strongly non-linear dynamics. Moreover, our method enables data-driven solution of optimal control problems involving non-linear dynamics, with some interesting implications on controllability.

Key words. Koopman Operator, Non-autonomous Dynamics, Machine Learning, Invariant Subspace, Control

MSC codes. 47N70, 37N35, 49M99

1. Introduction. Parametric models play a crucial role in modelling dynamical processes, allowing one to analyze, optimize, and control them by capturing the relationship between system behaviour and input parameters. However, in many scenarios, complete knowledge of the dynamics may be unavailable and only trajectory data is accessible. Discovering the relationship between states and parameters by data-driven approaches is particularly challenging, especially in non-linear and high-dimensional systems. The Koopman operator approach [30], initially developed to convert autonomous non-linear dynamical systems into infinite-dimensional linear systems has emerged as a powerful tool for spectral analysis and identification of significant dynamic modes for autonomous systems [50, 28, 9, 44]. Various data-driven strategies, such as dynamic mode decomposition (DMD) [51, 50, 61] and extended DMD (EDMD) [64, 63], have been proposed for approximating the Koopman operator from data.

In this study, we propose an extension of Koopman operator’s application to

*

Funding: This research is part of the programme DesCartes and is supported by the National Research Foundation, Prime Minister’s Office, Singapore under its Campus for Research Excellence and Technological Enterprise (CREATE) programme. GY is supported by the National Research Foundation, Singapore, under the NRF fellowship (project No. NRF-NRFF13-2021-0005). The work of IGK is partially supported by the US Department of Energy and the US Air Force Office of Scientific Research. The work of MK is supported by the AI Interdisciplinary Institute ANITI funding, through the French “Investing for the Future PIA3” program under the Grant agreement n° ANR-19-PI3A-0004. This work is also co-funded by the European Union under the project ROBOPROX (reg. no. CZ.02.01.01/00/22.008/0004590).

[†]Department of Mathematics, National University of Singapore, 117543, Singapore (guoyue@u.nus.edu).

[‡]CNRS, LAAS, 7 avenue du colonel Roche, F-31400 Toulouse, France; Faculty of Electrical Engineering, Czech Technical University in Prague, Prague, Czech Republic; CNRS@CREATE LTD, 1 Create Way, CREATE Tower, 138602, Singapore (korda@laas.fr).

[§]Department of Chemical and Biomolecular Engineering, Johns Hopkins University, 3400 North Charles Street Baltimore, MD 21218, USA (yannisk@jhu.edu).

[¶]Department of Mathematics & Institute for Functional Intelligent Materials, National University of Singapore, 117543, Singapore; CNRS@CREATE LTD, 1 Create Way, CREATE Tower, 138602, Singapore (qianxiao@nus.edu.sg).

parametric *discrete-time* dynamics. To parametrize and approximate a parameter-dependent Koopman operator within an invariant subspace, we propose a learning-based method that combines the ideas in extended dynamic mode decomposition with dictionary learning (EDMD-DL) [34] and a general form of the parametric Koopman operator that is expanded on a set of *fixed* basis functions [62]. Our approach is suited for high-dimensional and strongly non-linear systems, and for both forward non-autonomous prediction problems and optimal control problems. Currently, there are many works on the incorporation of parameters in Koopman decomposition, but they are mostly limited to linear or bilinear dynamics in the observable space. Some studies focus on the linear form related to DMD with controls [47, 48] and EDMD with control [31], which has been applied to system identification [3, 15, 55, 35, 41], especially for soft robotic system [21, 6]. Recent studies have introduced various parametric adaptations to DMD, utilizing interpolation techniques for enhancing predictions in non-linear dynamics and across parameter spaces. In [57], the authors employ Radial Basis Function (RBF) interpolation for mapping parameters to time snapshots, enabling the incorporation of new parameters with either exact DMD or Kernel DMD. A distinct approach is introduced in [1], where DMD is learned for various parameters, and predictions for new parameters are made by modelling the relationship between parameters and their outcomes. Another DMD-based approach emphasizes deriving parameter information from the nearest data points, utilizing methods such as Lagrangian interpolation to improve prediction precision [26]. Our approach learns a *non-linear* representation of parameters and states within a linear framework, bypassing the need for additional computations like nearest neighbourhood identification and the limitation of the linearity of DMD. This strategy ensures robust continuity and adaptability in the parameter domain, offering effective generalization to new parameter scenarios. When the system exhibits deviation from linearity, a bilinear form of Koopman dynamics has been explored for adaptation [58, 18, 46, 7, 14, 56]. However, these approaches may not be able to address applications involving strongly non-linear parametric dynamics. We tackle this problem by embedding the non-linear parameter dependence directly into the finite-dimensional approximation of the Koopman operator, which acts over a constructed common invariant subspace *over the entire parameter space*. Naturally, the simultaneous construction of a parametric Koopman operator approximation *as well as a common* invariant subspace is challenging. To resolve this, we leverage the function approximation capabilities of neural networks and jointly train them from data. We show that our approach can capture intricate non-linear relationships between high-dimensional states and parameters, and can be used to solve, in a data-driven way, both parametrically varying prediction problems and optimal control problems.

The paper is organized as follows: In [section 2](#), we introduce our definition of parametric dynamical systems and the parametric Koopman operator. In [section 3](#), we present our method for finding a common invariant subspace and approximating the projected Koopman operator on this subspace. In [section 4](#), we demonstrate, using a variety of numerical examples, that our approach provides performance improvements over existing methods.

2. Koopman operator family for parametric dynamical systems. We begin by introducing the basic formulation of Koopman operator analysis for parametric dynamical systems that we adopt throughout this paper.

2.1. Parametric dynamical systems. Let (X, \mathcal{S}, m) , with $X \subseteq \mathbb{R}^{N_x}$ be a finite measure space where \mathcal{S} is the Borel σ -algebra and m is a measure on (X, \mathcal{S}) .

Consider a set $U \subseteq \mathbb{R}^{N_u}$ of parameters, and a corresponding parametric family of transformations $X \rightarrow X$

$$(2.1) \quad \mathcal{F} = \{\mathbf{f}(\cdot, \mathbf{u}) : \mathbf{u} \in U\}.$$

This family of transformations can be used to define parametric discrete-time dynamics ($\mathbf{x}_{n+1} = \mathbf{f}(\mathbf{x}_n, \mathbf{u})$, $n = 0, 1, \dots$) where \mathbf{u} remains static, or control systems ($\mathbf{x}_{n+1} = \mathbf{f}(\mathbf{x}_n, \mathbf{u}_n)$, $n = 0, 1, \dots$) where \mathbf{u}_n changes in discrete steps dynamically. In both cases, at each time instant n the state evolves according to one member of the family $\{\mathbf{x} \mapsto \mathbf{f}(\mathbf{x}) : \mathbf{f} \in \mathcal{F}\}$. We note that such discrete dynamics can be also used to model continuous ones via time-discretization. In the case of continuous control systems, we shall only consider those controls that can be well-approximated by piecewise constant-in-time functions, e.g. essentially bounded controls.

2.2. Parametric Koopman operators. The main idea of the Koopman operator approach lies in understanding the *evolution of observables over time*, rather than the evolution of individual states themselves. To this end, let us consider the space of square-integrable observables

$$(2.2) \quad L^2(X, m) = \{\phi : X \rightarrow \mathbb{R} : \|\phi\|_{L^2(X, m)} < \infty\}$$

with the inner product $\langle \phi, \psi \rangle = \int_X \phi(\mathbf{x})\psi(\mathbf{x})m(d\mathbf{x})$ and norm $\|\phi\|_{L^2(X, m)} = |\langle \phi, \phi \rangle|^{\frac{1}{2}}$. When there is no ambiguity, we will write L^2 to mean $L^2(X, m)$. It is worth noting that a similar definition can also be provided for complex observables, but the analysis and experiments in this study focus on real-valued observables. Therefore, we use \mathbb{R} as the range of observables. Given any observable $\phi \in L^2$, for each \mathbf{u} , we have $\phi(\mathbf{x}_{n+1}) = \phi(\mathbf{f}(\mathbf{x}_n, \mathbf{u})) = \phi \circ \mathbf{f}(\mathbf{x}_n, \mathbf{u})$, where the composition is in the \mathbf{x} variable. Hence, the dynamics $\mathbf{x}_{n+1} = \mathbf{f}(\mathbf{x}_n, \mathbf{u})$ induces a dynamics on the space of the observables $\phi(\mathbf{x}_{n+1}) = \mathcal{K}(\mathbf{u})\phi(\mathbf{x}_n)$, where $\mathcal{K}(\mathbf{u}) : L^2 \rightarrow L^2$ is the *parametric Koopman operator*, defined by

$$(2.3) \quad \mathcal{K}(\mathbf{u})\phi(\mathbf{x}) \triangleq \phi \circ \mathbf{f}(\mathbf{x}, \mathbf{u}).$$

For each \mathbf{u} , $\mathcal{K}(\mathbf{u})$ is linear since $\mathcal{K}(\mathbf{u})(a\phi_1 + b\phi_2) = a\mathcal{K}(\mathbf{u})\phi_1 + b\mathcal{K}(\mathbf{u})\phi_2$ for $a, b \in \mathbb{R}$ and $\phi_1, \phi_2 \in L^2$. **Proposition 2.1** gives conditions for $\{\mathcal{K}(\mathbf{u})\}$ to be a well-defined family of bounded linear operators on $L^2 \rightarrow L^2$, which we denote by $\mathcal{B}(L^2)$. This follows directly from known results in autonomous systems [53], but we include its proof in **Appendix A** for completeness. We hereafter assume that these conditions are satisfied.

PROPOSITION 2.1. *Let $\mathcal{F} = \{\mathbf{f}(\cdot, \mathbf{u}) : \mathbf{u} \in U\}$ be a family of non-singular transformations on X , i.e., for every $S \in \mathcal{S}$, $m(\mathbf{f}^{-1}(\cdot, \mathbf{u})(S)) = 0$ whenever $m(S) = 0$. Then, $\mathcal{K}(\mathbf{u}) \in \mathcal{B}(L^2)$ if and only if there exists $b_{\mathbf{u}} > 0$ such that $m(\mathbf{f}^{-1}(\cdot, \mathbf{u})(S)) \leq b_{\mathbf{u}}m(S)$ for every $S \in \mathcal{S}$.*

Just like the parametric family of transformations $\{\mathbf{f}(\cdot, \mathbf{u})\}$, the Koopman operator family $\{\mathcal{K}(\mathbf{u})\}$ can drive both discrete-time parametric dynamics ($\phi_{n+1} = \mathcal{K}(\mathbf{u})\phi_n$) or discrete-time control systems ($\phi_{n+1} = \mathcal{K}(\mathbf{u}_n)\phi_n$), both now in the L^2 space of observables.

3. Invariant subspace and finite-dimensional approximation of Koopman operator. The central challenge of the Koopman approach is how to efficiently find an invariant subspace and approximate a projected Koopman operator acting

on this subspace. To achieve this for *parametric* cases, we generalize the Extended Dynamic Mode Decomposition with Dictionary Learning (EDMD-DL) [34], but the family of Koopman evolution operators are approximated by a matrix-valued function of the parameter, acting on an invariant subspace of observables spanned by *parameter-independent dictionaries*. In our approach, both the evolution matrix and the dictionary are parameterized by neural networks and jointly trained. Then, we can use the trained parametric Koopman operator on prediction and control problems defined on the invariant subspace.

3.1. Numerical methods for autonomous dynamics. We first recall the method in [34] to find an invariant subspace and approximate the Koopman operator on this subspace for autonomous (non-parametric) dynamical systems of the form

$$(3.1) \quad \begin{aligned} \mathbf{x}_{n+1} &= \mathbf{f}(\mathbf{x}_n), \\ \mathbf{y}_n &= \mathbf{g}(\mathbf{x}_n). \end{aligned}$$

Here, \mathbf{g} is a length- N_y vector of L^2 observable functions \mathbf{y} , whose evolution we are interested in modelling. The goal is then to find a finite-dimensional subspace $H \subset L^2$ that contains the components of \mathbf{g} , and moreover is *invariant* under the action of the Koopman operator $\mathcal{K}(\phi) = \phi \circ \mathbf{f}$, i.e. $\mathcal{K}(H) \subset H$, at least approximately. A simple but effective method [63] is to build H as the span of a set of dictionary functions $\{\psi_1, \psi_2, \dots, \psi_{N_\psi}\}$ where $\psi_i \in L^2(X, m)$, with $\psi_i = g_i$ for $i = 1, \dots, N_y$. Let us write $\Psi := (\psi_1, \psi_2, \dots, \psi_{N_\psi})^T$ and consider the subspace $\text{span}(\Psi) = \{\mathbf{a}^T \Psi : \mathbf{a} \in \mathbb{R}^{N_\psi}\}$. For each $\phi \in \text{span}(\Psi)$, we can write $\mathcal{K}\phi = \mathbf{a}^T \mathcal{K}\Psi = \mathbf{a}^T \Psi \circ \mathbf{f}$. If we assume that $\mathcal{K}(\text{span}(\Psi)) \subset \text{span}(\Psi)$, which is equivalent to the existence of $\mathbf{k}_i \in \mathbb{R}^{N_\psi}$ such that $\mathcal{K}\psi_i = \mathbf{k}_i^T \Psi$ for each $i = 1, 2, \dots, N_\psi$, then the Koopman operator \mathcal{K} can be represented by a finite dimensional matrix $K \in \mathbb{R}^{N_\psi \times N_\psi}$ whose i^{th} row is \mathbf{k}_i^T . In this case, we call $\text{span}(\Psi)$ a *Koopman invariant subspace*.

In practice, the matrix K , and the invariant subspace, can only be found as approximations. Concretely, one first takes a sufficiently large, fixed dictionary Ψ . From the dynamical system (3.1), we collect data pairs $\{\mathbf{x}_{n+1}^{(m)}, \mathbf{x}_n^{(m)}\}_{n,m=0}^{N-1, M-1}$, where $\mathbf{x}_{n+1}^{(m)} = \mathbf{f}(\mathbf{x}_n^{(m)})$ and $\mathbf{x}_n^{(m)}$ is the state on the m^{th} trajectory at time n . Then, an approximation of the Koopman operator on this subspace is computed via least squares

$$(3.2) \quad \hat{K} = \underset{K \in \mathbb{R}^{N_\psi \times N_\psi}}{\text{argmin}} \sum_{n,m=0}^{N-1, M-1} \|\Psi(\mathbf{x}_{n+1}^{(m)}) - K\Psi(\mathbf{x}_n^{(m)})\|^2.$$

Assuming the data is in a general position, the solution is guaranteed to be unique when the number of data pairs is at least equal to or larger than the dimension of the dictionary Ψ . Otherwise, a regularizer can be incorporated to ensure uniqueness.

Although the solution for (3.2) is straightforward, choosing the dictionary set Ψ is a non-trivial task, especially for high-dimensional dynamical systems [32, 64]. Consequently, machine learning techniques have been employed to overcome this limitation by learning an adaptive dictionary from data [34, 13, 38, 42, 43, 59]. The simplest approach [34] is to parametrize Ψ using a neural network with trainable weights θ_ψ , so that $\Psi(\cdot; \theta_\psi)$ is a *set of trainable dictionary functions*. The method iteratively updates θ_ψ and the matrix K by minimizing the loss function

$$(3.3) \quad L(K, \theta_\psi) = \sum_{n,m=0}^{N-1, M-1} \|\Psi(\mathbf{x}_{n+1}^{(m)}; \theta_\psi) - K\Psi(\mathbf{x}_n^{(m)}; \theta_\psi)\|^2,$$

over K and θ_ψ . We note that other losses can be used to promote different properties of the learned invariant subspace. For example, one may focus on minimizing the worst-case error [22], instead of the average error considered above.

3.2. Numerical methods for parametric dynamics. We now extend the previous algorithm to the parametric case

$$(3.4) \quad \begin{aligned} \mathbf{x}_{n+1} &= \mathbf{f}(\mathbf{x}_n, \mathbf{u}_n), \\ \mathbf{y}_n &= \mathbf{g}(\mathbf{x}_n). \end{aligned}$$

This includes the static setting by setting \mathbf{u}_n to be constant over the n -th time interval. Now, the natural extension of the method for autonomous dynamics is to

1. Find a dictionary Ψ whose elements are in L^2 (the first N_y of which are \mathbf{g}) such that $\text{span}(\Psi)$ is invariant under $\mathcal{K}(\mathbf{u})$ for all $\mathbf{u} \in U$.
2. Construct a $N_\Psi \times N_\Psi$ matrix-valued function $K(\mathbf{u})$ that approximates $\mathcal{K}(\mathbf{u})$ on $\text{span}(\Psi)$.

However, the validity of this procedure is not immediately obvious, since finding a common invariant subspace for all parameters, even approximately, may be challenging. We first show in Proposition 3.1 below that this is theoretically possible under appropriate conditions, and subsequently in section 4 that it can be achieved in practice. In the following, $C_b(X)$ denotes the space of continuous bounded functions on X and $C(U)$ denotes the space of continuous functions on U . We also assume that the state space X is a finite measure space and consider observables in $C_b(X) \subset L^2(X, m)$. The proof is found in Appendix B.

PROPOSITION 3.1. *Let U be compact and X be a finite measurable space, the observables of interest \mathbf{g} satisfy $g_j \in C_b(X)$ and suppose that $f(\mathbf{x}, \cdot) : U \rightarrow X$ is continuous for m -a.e. $\mathbf{x} \in X$. Then, for any $\varepsilon > 0$, there exists a positive integer $N_\psi > 0$, a dictionary $\Psi = \{\psi_1, \dots, \psi_{N_\psi}\}$ with $\psi_i \in L^2$, a set of vectors $\{\mathbf{a}_j \in \mathbb{R}^{N_\psi} : j = 1, \dots, N_y\}$, and a continuous function $K : U \rightarrow \mathbb{R}^{N_\psi \times N_\psi}$ such that $g_j = \mathbf{a}_j^T \Psi$ and for all $\mathbf{u} \in U$, we have $\|\mathcal{K}(\mathbf{u})g_j - \mathbf{a}_j^T K(\mathbf{u})\Psi\| \leq \varepsilon$.*

Proposition 3.1 shows that it is possible to construct a parameter-independent subspace such that the one-step evolution of the observables are approximately closed, and that the projected Koopman operator on this subspace is a continuous function. In particular, this suggests that we can use neural networks to approximate both the dictionary elements as $\Psi(\cdot; \theta_\psi) : X \rightarrow \mathbb{R}^{N_\psi}$, and the projected Koopman operator as $K(\mathbf{u}; \theta_K) : U \rightarrow \mathbb{R}^{N_\psi \times N_\psi}$. As before, we fix the first N_y entries in Ψ to be \mathbf{g} , while the remaining $N_\psi - N_y$ entries are learned. The observables \mathbf{g} can be recovered by $\mathbf{g} = B\Psi$ with

$$(3.5) \quad B = \begin{bmatrix} I_{N_y} & O_{N_y \times (N_\psi - N_y)} \end{bmatrix}_{N_y \times N_\psi},$$

where I_{N_y} is a $N_y \times N_y$ identity matrix and $O_{N_y \times (N_\psi - N_y)}$ is a $N_y \times (N_\psi - N_y)$ zero matrix. We train Ψ and K by collecting data triples $\{\mathbf{x}_{n+1}^{(m)}, \mathbf{x}_n^{(m)}, \mathbf{u}_n^{(m)}\}_{n,m=0}^{N-1, M-1}$, where $\mathbf{x}_{n+1}^{(m)} = \mathbf{f}(\mathbf{x}_n^{(m)}, \mathbf{u}_n^{(m)})$, $\mathbf{x}_n^{(m)}$ and $\mathbf{u}_n^{(m)}$ are states and parameters on the m th trajectory at time n . We then minimize the loss function

$$(3.6) \quad L(\theta_K, \theta_\psi) = \sum_{n,m=0}^{N-1, M-1} \|\Psi(\mathbf{x}_{n+1}^{(m)}; \theta_\psi) - K(\mathbf{u}_n^{(m)}; \theta_K)\Psi(\mathbf{x}_n^{(m)}; \theta_\psi)\|^2,$$

over θ_K and θ_ψ . A graphical representation of our approach to learn parametric Koopman dynamics, which we call PK-NN, is shown in Figure 1 and the training workflow is summarised in Algorithm 3.1. The weights are initialized using the Glorot Uniform initializer [16]. The architecture of NN_K consists of a multi-layer, fully connected neural network, while NN_ψ is a residual network to improve optimization performance. We use the hyperbolic tangent as the activation function for all hidden layers and a dense layer without activations as the output layers. The detailed choices of model sizes differ by application and are included in the corresponding experimental sections. The Adam optimizer is used for all experiments [29].

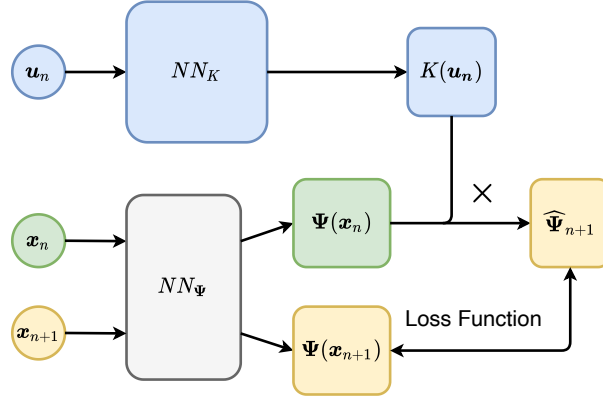


Fig. 1: The neural network architecture of PK-NN. The trainable parameters of $K(\mathbf{u}; \theta_K)$ are integrated within the structure of NN_K , and a distinct neural network NN_Ψ is used to parametrize the dictionaries $\Psi(\mathbf{x}; \theta_\psi)$.

Algorithm 3.1 Parametric Koopman decomposition with neural networks (PK-NN)

Data: $\{\mathbf{x}_{n+1}^{(m)}, \mathbf{x}_n^{(m)}, \mathbf{u}_n^{(m)}\}_{n,m=0}^{N-1,M-1}$

Initialize: Random (θ_K, θ_ψ) .

Set learning rate $\delta > 0$; tolerance $\varepsilon > 0$; optimizer `Opt`.

while $L(\theta_K, \theta_\psi) > \varepsilon$ **do**

 Evaluate $L(\theta_K, \theta_\psi) = \sum_{n,m=0}^{N-1,M-1} \|\Psi(\mathbf{x}_{n+1}^{(m)}; \theta_\psi) - K(\mathbf{u}_n^{(m)}; \theta_K) \Psi(\mathbf{x}_n^{(m)}; \theta_\psi)\|^2$;

 Update trainable parameters (θ_K, θ_ψ) using `Opt` to minimize $L(\theta_K, \theta_\psi)$;

end while

We close the presentation of our approach with a discussion on related methodologies. We begin with neural network architectural design. For the dictionary network Ψ , we essentially follow the approaches in [34, 65] by incorporating \mathbf{g} into Ψ via linear transformations, so that \mathbf{g} can be recovered by a linear operation (e.g. $\mathbf{g} = B\Psi$). When \mathbf{g} is high-dimensional, one may alternatively employ non-linear variants and recover \mathbf{g} from Ψ with a trained decoder network [13, 38, 42, 43, 59]. These variants can be readily incorporated into our parametric framework. For the projected Koopman operator network K , our method can be viewed as an adaptive version of that introduced in [62], which writes $K(\mathbf{u})$ as a linear combination $\sum_i^{N_K} K_i h_i(\mathbf{u})$, with h_i fixed and K_i are fitted from data. If we use a fully connected network to parametrize K , then our method generalizes this approach by also training h_i . More generally,

our method allows for alternative architectures for K , beyond fixed or adaptive basis expansions.

Let us further contrast our approach with other existing Koopman operator based approaches for non-autonomous systems. The first class of methods posits a linear (or Bilinear) system in the observable space [47, 58, 31, 33], e.g. $\Psi_{n+1} = A\Psi_n + B\mathbf{u}_n$. These have the advantage of linearity, but as we will show in section 4 that the linearity (or bi-linearity) assumption maybe too restrictive for some applications. These can be seen as a special case of our approach with $\mathcal{K}(\mathbf{u})$ affine in \mathbf{u} . A recent generalization of these methods [12] considers a non-linear transformation of the parameter \mathbf{u} , i.e., systems of the form $\Psi_{n+1} = A\Psi_n + B\Phi(\mathbf{u}_n)$. Another class of methods regard a parametric dynamical system as an autonomous one in the extended state space $X \times U$, in the most general case, will result in parameter-dependent invariant subspaces (i.e. $\Psi = \Psi(\mathbf{x}, \mathbf{u})$), unless some further linearity assumptions are introduced [48]. This framework has been applied to control problems [52]. Alternatively, the recent work [23] posits a separable form for the dictionaries $\Psi(\mathbf{x}, \mathbf{u}) = G(\mathbf{u})H(\mathbf{x})$. If such a form exists, then $H(\mathbf{x})$ spans a common invariant subspace. In this sense, our method (Proposition 3.1) gives a different approach to constructing a common invariant subspace, at least approximately.

3.3. Parametric Koopman analysis for prediction and control. After PK-NN is trained, we can leverage it to solve prediction and control problems in the same family of parametric dynamics.

Prediction problems.. We start with prediction problems. In this scenario, an initial value \mathbf{x}_0 and one choice of constant parameter \mathbf{u} or a sequence of parameters $\{\mathbf{u}_n\}$ are given. The goal is to predict the sequence of observable values $\{\mathbf{g}(\mathbf{x}_n)\}$ generated by the underlying dynamics. Recall that \mathbf{g} is a given vector-valued observable function, which by design lies in the span of Ψ , i.e. $\mathbf{g} = B\Psi$ where B is defined in (3.5). The prediction algorithm is summarized in Algorithm 3.2 for the time-varying parameters case, and the constant parameter case simply replaces all \mathbf{u}_n with \mathbf{u} .

Algorithm 3.2 Prediction by PK-NN.

Initial state: \mathbf{x}_0 . Parameters: $\{\mathbf{u}_n\}_{n=0}^{N-1}$.
 $\hat{\Psi}_0 = \Psi(\mathbf{x}_0)$.
for $0 \leq n \leq N - 1$ **do**
 $\hat{\Psi}_{n+1} = K(\mathbf{u}_n)\hat{\Psi}_n$;
 $\hat{\mathbf{g}}_{n+1} = B\hat{\Psi}_{n+1}$;
end for
Output: $\{\hat{\mathbf{g}}_n\}_{n=1}^N$.

Optimal control problems.. In the opposite direction, PK-NN enables us to solve a variety of inverse-type problems, where the goal is to perform inference or optimization on the space of parameters U , e.g. system identification. In this work, we focus on the particularly challenging class of such problems in the form of optimal control problems. Concretely, we consider the discrete Bolza control problem whose cost

function depends on the observable values

$$(3.7) \quad \begin{aligned} \min_{\{\mathbf{u}_n\}_{n=0,1,\dots,N-1}} \quad & J[\{\mathbf{u}_n\}] = \Phi(\mathbf{g}(\mathbf{x}_N)) + \sum_{n=1}^N L_n(\mathbf{g}(\mathbf{x}_n), \mathbf{u}_{n-1}) \\ \text{s.t.} \quad & \mathbf{x}_{n+1} = \mathbf{f}(\mathbf{x}_n, \mathbf{u}_n). \end{aligned}$$

Here the initial condition, the terminal cost Φ and the running costs L_n are given, but the dynamics \mathbf{f} is unknown. Note that in the fully observed case ($\mathbf{g}(\mathbf{x}) = \mathbf{x}$), this is a standard Bolza problem. After the construction of Ψ and K from data, PK-NN transforms (3.7) into

$$(3.8) \quad \begin{aligned} \min_{\{\mathbf{u}_n\}_{n=0,1,\dots,N-1}} \quad & J[\{\mathbf{u}_n\}] = \Phi(B\hat{\Psi}_N) + \sum_{n=1}^N L_n(B\hat{\Psi}_n, \mathbf{u}_{n-1}) \\ \text{s.t.} \quad & \hat{\Psi}_{n+1} = K(\mathbf{u}_n)\hat{\Psi}_n, \\ & \hat{\Psi}_0 = \Psi(\mathbf{x}_0), \end{aligned}$$

which can be solved using standard optimization libraries. A concrete example is the tracking problem [54, 31], with the objective of achieving precise following of a desired reference observable trajectory $\{\mathbf{r}_n\}_{n=0}^N$. In this case, $\Phi \equiv 0$ and $L_n(\mathbf{y}, \mathbf{u}) = \|\mathbf{y} - \mathbf{r}_n\|^2$.

It is of particular importance to discuss the case where the control problem does not concern the full state \mathbf{x} , but only some pre-defined observables of it. A simple example is a tracking problem that only requires tracking the first coordinate of the state. In this case, the dictionaries Ψ are only required to include the map $\mathbf{g}(\mathbf{x}) = x_1$. Thus, one can interpret our approach as a Koopman-operator-assisted model reduction method for data-driven control.

In the literature, there exist control approaches which limit to a finite number of control choices, such as those described in [45] and [4]. These transform the dynamic control problem into a set of autonomous representations and time-switching optimization problems. In particular, [4] leverages input-parameterized Koopman eigenfunctions to handle systems with finite control options, embedding the control within the Koopman eigenfunctions to solve the control problems for the system with fixed points. In contrast, PK-NN allows for control values to be chosen arbitrarily within a predefined range without being restricted to a set of finite, predetermined options. This feature gives our approach greater flexibility in tackling various control problems.

Compared to existing data-driven approaches, there are some distinct advantages to transforming (3.7) into (3.8). First, compared with methods that learn linear or bilinear control systems in the observable space [47, 58], the transformed problem (3.8) is valid for general dynamics, where \mathbf{f} may be strongly non-linear in both the state and the control. In these cases, we observe more significant improvements using our method (See subsection 4.2). Second, we contrast with the alternative approach of first learning \mathbf{f} in (3.7) using existing non-linear system identification techniques [10, 37, 60], and then applying optimal control algorithms directly to (3.7). While this approach is feasible for low-dimensional systems, it becomes inefficient when dealing with high-dimensional non-linear systems, where the control objectives only depend on a few low-dimensional observables. Our method can avoid the expensive identification of high-dimensional dynamics and the subsequent even more expensive optimal control problem in high dimensions. Instead, we parsimoniously construct a low-dimensional control system in the form of (3.8), on which the reduced control problem can be

easily solved (See tracking the mass and momentum of Korteweg-De Vries (KdV) equation in [subsection 4.2](#)).

3.4. PK-NN and non-linear controllability. We conclude with a discussion on the interesting subject of controllability. For control problems, and in particular tracking problems, it is desirable that the constructed data-driven state dynamics should be controllable, i.e. the initial state can be driven to an arbitrary target state, at least locally. This gives the system flexibility to track a given trajectory. The controllability rank condition in the lifting space of the Koopman operator analysis with a linear dependence on the control is addressed in [8]. Nevertheless, such linear models (as we show in [section 4](#)) have limited modelling capabilities in the general non-linear setting, prompting us to consider the controllability of PK-NN type Koopman dynamics. In particular, we demonstrate that the dynamics (3.8) has the special property that controllability conditions are readily checked, and may even be algorithmically enforced.

We discuss this in the context where the dynamics $\mathbf{x}_{n+1} = \mathbf{f}(\mathbf{x}_n, \mathbf{u}_n)$ is a discretization of a differential equation $\dot{\mathbf{x}} = \mathbf{f}(\mathbf{x}, \mathbf{u})$ with initial condition $\mathbf{x}(0) = \mathbf{x}_0$. We assume $\mathbf{f}(\mathbf{x}, \mathbf{u})$ is continuous in \mathbf{u} and Lipschitz continuous in \mathbf{x} across the entire domain. This assumption guarantees the existence of a unique solution of $\dot{\mathbf{x}} = \mathbf{f}(\mathbf{x}, \mathbf{u})$ by the Picard–Lindelöf theorem and inherently ensures forward completeness [2, 17]. Thus, the discrete system $\mathbf{x}_{n+1} = \mathbf{f}(\mathbf{x}_n, \mathbf{u}_n)$ effectively approximates the continuous system by defining $\mathbf{f}(\mathbf{x}_n, \mathbf{u}_n)$ as the solution to $\dot{\mathbf{x}} = \mathbf{f}(\mathbf{x}, \mathbf{u})$ with $\mathbf{x}(0) = \mathbf{x}_n$ and with $\mathbf{u}(t) = \mathbf{u}_n$ being constant over a given sampling interval Δt . If the continuous system is controllable, the controllability of the discrete system can be approximately guaranteed within any arbitrary error. A classical sufficient condition for controllability is a corollary of the Chow-Rashevsky theorem [11, 49]: if the family $\mathcal{F} = \{\mathbf{f}(\cdot, \mathbf{u}) : \mathbf{u} \in U\}$ is smooth and symmetric (meaning that $-\mathbf{f} \in \mathcal{F}$ if $\mathbf{f} \in \mathcal{F}$), then the system is controllable with piecewise constant control if $\dim \text{Lie}_{\mathbf{x}} \mathcal{F} = d$ for each \mathbf{x} , where $\text{Lie}_{\mathbf{x}} \mathcal{F}$ is the span of the Lie algebra generated by \mathcal{F} at \mathbf{x} . While useful, this condition is difficult to check for a given \mathbf{f} , as it requires the generation of Lie algebras at *every* point in the state space, unless each member of \mathcal{F} is linear. This is the fundamental difficulty towards ensure, or even verifying the controllability of non-linear systems.

However, it turns out that controllability is much easier to check for the transformed system under parametric Koopman operator analysis. Given observable $\phi \in C_b$, for each \mathbf{u} , the Koopman operator is well-defined and can be considered as strongly continuous semigroups $(\mathcal{S}^t(\mathbf{u}))_{t \geq 0}$ with $\mathcal{S}^t(\mathbf{u})\phi(\mathbf{x}_0) = \phi(\mathbf{x}(t))$, $\mathcal{S}^0(\mathbf{u})\phi(\mathbf{x}) = \phi(\mathbf{x})$ [25, 39]. There exists a dense subset D (such as C^∞) of $C_b(X)$ such that $\dot{\phi} = \lim_{t \rightarrow 0^+} \frac{\mathcal{S}^t(\mathbf{u})\phi - \phi}{t} \triangleq \tilde{\mathcal{K}}(\mathbf{u})\phi$ exists in the strong sense for $\phi \in D$. This defines the Koopman generator $\tilde{\mathcal{K}}(\mathbf{u}) : D \rightarrow C_b(X)$, which is the time derivative over the evolution of the observables. We assume that ϕ is approximately in a finite-dimensional subspace, and the components in the dictionary Ψ span this subspace. The continuous analogue to (3.8) is thus $\dot{\Psi} = \tilde{K}(\mathbf{u})\Psi$ where $\tilde{K}(\mathbf{u})$ is the projected Koopman generator onto the dictionary Ψ . Concretely, we may compute the corresponding projected Koopman generator for the continuous system as $\tilde{K}(\mathbf{u}) = \frac{K(\mathbf{u}) - I}{\Delta t}$ where I is an identity matrix. Furthermore, we can extend this to a finite number of observables ϕ_i 's which can be represented in this subspace. Controllability in the continuous system $\dot{\Psi} = \tilde{K}(\mathbf{u})\Psi$ ensures these observables ϕ_i 's are also controllable. Then, the control family $\mathcal{F} = \{\tilde{K}(\mathbf{u})(\cdot) : \mathbf{u} \in U\}$ is now a family of *linear* functions. Therefore, the controllability conditions can be checked at one (any) state, and automatically carries over to all states. We note that this notion of controllability is not over the

original state space, but over the (approximately) invariant subspace spanned by Ψ . In this sense, we can understand the parametric Koopman approach as one that constructs an invariant subspace of observables with the property that *controllability in this subspace at any point carries over to the whole subspace* – a desirable property of linear control systems.

One way to verify controllability is as follows. Let $\text{Lie}_{\mathbf{x}}^{(0)}\mathcal{F} \triangleq \text{span}\{\tilde{K}(\mathbf{u})\mathbf{x} : \mathbf{u} \in U\}$. We know that $\text{Lie}_{\mathbf{x}}^{(0)}\mathcal{F} \subseteq \text{Lie}_{\mathbf{x}}\mathcal{F}$. Then, $\dim \text{Lie}_{\mathbf{x}}\mathcal{F} = d$ can be guaranteed by $\dim \text{Lie}_{\mathbf{x}}^{(0)}\mathcal{F} = d$, which is equivalent to: for any non-zero vectors $\mathbf{v}_1, \mathbf{v}_2 \in \mathbb{R}^d$, there exists $\mathbf{u}_j \in U$ such that $\mathbf{v}_1^T \tilde{K}(\mathbf{u}_j) \mathbf{v}_2 \neq 0$. This can be ensured if the flattened matrices $\{\tilde{K}(\mathbf{u}) : \mathbf{u} \in U\}$ do not lie in a proper subspace. Algorithmically, we collect a large sample of parameters \mathbf{u}_i , $i = 1, 2, \dots, N$, flatten each matrix $\tilde{K}(\mathbf{u}_i) \in \mathbb{R}^{d \times d}$ into a vector $\mathbf{k}_i \in \mathbb{R}^{d^2}$ and concatenate all \mathbf{k}_i s as a $d^2 \times N$ matrix

$$(3.9) \quad C = [\mathbf{k}_1, \mathbf{k}_2, \dots, \mathbf{k}_N].$$

The system is controllable if the rank of $C = d^2$. We show in [subsection 4.2](#) that this can be readily checked for a learned PK-NN system, and moreover, that it may guide architecture designs for $\mathbf{u} \mapsto K(\mathbf{u})$ that promote controllability, yielding an approach that finds a parsimonious controllable dynamics in the observable space. It should be noted that although this rank condition is sufficient to guarantee the controllability of the observables, it is not necessary when the observables Ψ form a manifold. Investigating the model structure design and the controllability of the manifold presents an interesting future research direction.

4. Numerical experiments. In this section, we present numerical results on a variety of prediction and control problems. We evaluate various baseline methods, noting that some of these overlap in different aspects of the comparison. For convenience, we introduce a standard format to refer to these methods in [Table 1](#). The code to reproduce these experiments are found at [\[20\]](#).

Table 1: Summary of comparisons. “NN” stand for (residual) neural networks and “RBF” refers to dictionaries built from random radial basis functions. $u_{n,i}$ is the i^{th} component of \mathbf{u}_n .

Method Description	Ψ	Reference	Notation
$\mathbf{x}_{n+1} = K\mathbf{x}_n$ (Optimized DMD)	\mathbf{x}	[24]	M0
$\Psi(\mathbf{x}_{n+1}) = K\Psi(\mathbf{x}_n)$ (EDMD)	RBF	[63]	M1-RBF
	NN	[34]	M1-NN
$\Psi(\mathbf{x}_{n+1}) = A\Psi(\mathbf{x}_n) + B\mathbf{u}_n$	NN	[47]	M2
$\Psi(\mathbf{x}_{n+1}) = A\Psi(\mathbf{x}_n) + \sum_i B_i u_{n,i} \Psi(\mathbf{x}_n)$	NN	[58]	M3
$\Psi(\mathbf{x}_{n+1}) = \sum_{i=1}^M h_i(\mathbf{u}_n) K_i \Psi(\mathbf{x}_n)$ M is fixed and h_i are fixed polynomials	RBF	[62]	M4-RBF
	NN		M4-NN
$\Psi(\mathbf{x}_{n+1}) = K(\mathbf{u}_n)\Psi(\mathbf{x}_n)$	NN		Ours

We first demonstrate on prediction problems that PK-NN outperforms existing methods, including optimized DMD (M0), classical EDMD (M1-RBF) and EDMD

with dictionary learning (M1-NN) in [subsection 4.1.1](#), linear (M2) and bi-linear (M3) extensions to systems with parameters or control in [subsection 4.1.2](#) and a modified form of EDMD (M4) in [subsection 4.1.3](#). In the reverse direction, we show that PK-NN can solve data-driven optimal control problems in [subsection 4.2](#). Notably, our approach exhibits more significant improvements for problems with strong non-linearity or those involving high-dimensional states and parameters. Although the structure of the dictionary is detailed in the following paragraphs, here we highlight the dictionary is designed as $(1, \mathbf{x}, NN)^T$ by default. This consists of a constant element, the state \mathbf{x} and trainable components NN generated by neural networks, the same as the dictionary in [\[34\]](#). Furthermore, we construct $K(\mathbf{u})$ by assigning its first row to $(1, 0, \dots, 0)$, which constitutes one of the optimal choices for the first row in $K(\mathbf{u})$. We also provide a detailed discussion about selecting hyperparameters in PK-NN for different tasks in [Appendix H](#).

4.1. Prediction problems. Using [Algorithm 3.2](#), we test the performance of PK-NN on various forward prediction problems involving discretized parametric ordinary and partial differential equations. Here, the discrete-time step n corresponds to the physical time t_n of the continuous dynamics, and are equally spaced. We evaluate performance by the relative reconstruction error at t_n on the m^{th} trajectory is defined as

$$(4.1) \quad E^{(m)}(t_n) = \frac{\sqrt{\sum_{i=1}^n \|\hat{\mathbf{y}}_i^{(m)} - \mathbf{y}_i^{(m)}\|^2}}{\sqrt{\sum_{i=1}^n \|\mathbf{y}_i^{(m)}\|^2}},$$

where $\mathbf{y}_i^{(m)}$ is the true value of observables and $\hat{\mathbf{y}}_i^{(m)}$ is the predicted observables at t_i on the m^{th} trajectory. To evaluate the performance on M trajectories, we use the average $E(t_n) = \frac{1}{M} \sum_{m=1}^M E^{(m)}(t_n)$. If there is no special emphasis on the observation function, we set $\mathbf{g}(\mathbf{x}) = \mathbf{x}$, the full-state observable. With the state as the output at each step, we substitute the predicted state into the dictionary and multiply the dictionary by $K(\mathbf{u})$ to improve the stability of long-term predictions.

4.1.1. Improved accuracy and generalization over parameter independent Koopman dynamics. We first demonstrate that PK-NN can interpolate successfully in parameter space and improve upon naive training a separate (parameter-independent) Koopman dynamics for each observed \mathbf{u} using EDMD with dictionary learning (M1-NN) [\[34\]](#), EDMD with radial basis functions (M1-RBF) [\[63\]](#) and optimized DMD (M0) [\[24\]](#). We consider the parametric Duffing equation

$$(4.2) \quad \begin{aligned} \dot{x}_1 &= x_2, \\ \dot{x}_2 &= -\delta x_2 - x_1(\beta + \alpha x_1^2). \end{aligned}$$

To quantify performance, we use ν_1 to denote the number of trajectories for each set of fixed parameters $\mathbf{u} = (\delta, \alpha, \beta)$ and ν_2 to denote the number of different parameter configurations in the dataset. The baseline method trains ν_2 separate Koopman dynamics and chooses one such dynamic with parameter value being the nearest neighbour of the testing parameter for testing. On the other hand, PK-NN trains only one parametric Koopman dynamics that can interpolate over the space of the parameters \mathbf{u} and directly uses [Algorithm 3.2](#) to predict. For each configuration of ν_1 and ν_2 , training data is generated with trajectories initialized within the domain $[-2, 2] \times [-2, 2]$.

The parameters δ , α and β are randomly sampled from uniform distributions over the intervals $[0, 1]$, $[0, 2]$ and $[-2, 2]$ respectively. To ensure fairness, the total amount of training data $\nu_1 \times \nu_2 = 10000$ remains constant. For each trajectory, we observe the data points over 50 steps with $\Delta t = 0.25$, the same setting as the experiments in [34]. The dictionary NN_ψ is constructed as $(1, x_1, x_2, NN^T)^T$ where NN is a trainable 22-dimensional vector. This NN is the output of a 3-layer feed-forward ResNet with a width of 100 nodes in each layer. The dictionary by this design is employed in both PK-NN and M1-NN. For NN_K in PK-NN, we use a 3-layer fully connected neural network with width 256 before the output layer.

Our results, as shown in Figure 2, indicate that our method increasingly outperforms the other three approaches as ν_2 increases. This is because, while we have few representative trajectories per parameter instance (causing M1-NN and M1-RBF to fail), the interpolation in parameter space allows us to integrate information across trajectories with different parameter values, thus ensuring prediction fidelity and generalizability.

4.1.2. Improved performance on strongly non-linear problems. To see the performance of PK-NN on the problems with strong non-linearity, we test our method on the Van der Pol Mathieu equation [27]

$$(4.3) \quad \begin{aligned} \dot{x}_1 &= x_2, \\ \dot{x}_2 &= (k_1 - k_2 x_1^2)x_2 - (w_0^2 + 2\mu u^2 - \mu)x_1 + uk_3, \end{aligned}$$

where $k_1 = 2, k_2 = 2, k_3 = 1$ and $w_0 = 1$. The parameter u is designed to adjust both the parametric excitation $(2\mu u^2)x_1$ and the external excitation uk_3 . The value of the parameter $\mu > 0$ captures the non-linearity among $\mathbf{x} = (x_1, x_2)$ and u , and this non-linearity becomes more pronounced as the parameter μ increases. Training data consists of 500 trajectories with $\Delta t = 0.01$. Each trajectory spans 50 sampling time steps initialized from a uniformly randomly sampled point in $[-1, 1] \times [-1, 1]$. The parameter at each time step are also randomly sampled from uniform distributions over $[-1, 1]$. In this section, we consider the case where $\nu_1 = 1$ as in subsection 4.1.1, thus we do not compare with EDMD using RBF (M1-RBF) or NN (M1-NN), but instead with the linear Koopman with control approach (M2) [47]

$$(4.4) \quad \hat{\Psi}_{n+1} = A\hat{\Psi}_n + B\mathbf{u}_n,$$

and the bi-linear variant (M3) [58]

$$(4.5) \quad \hat{\Psi}_{n+1} = A\hat{\Psi}_n + \sum_i^{N_u} B_i u_{n,i} \hat{\Psi}_n,$$

where $u_{n,i}$'s are the components of vector $\mathbf{u}_n \in \mathbb{R}^{N_u}$ and A, B_i 's $\in \mathbb{R}^{N_\psi \times N_\psi}$. In experiments, to ensure the effect of dictionaries on state \mathbf{x} is the same, we use trainable dictionaries, which are built with the same network structure and the same dictionary number. The dictionary NN_ψ is $(1, x_1, x_2, NN^T)^T$ and the dimension of the trainable vector NN is 10. NN is designed by two hidden layers with width 64 and NN_K employs one hidden layer with width 128. In the experiments, we randomly initialize the dictionary and use the least squares method to get the initial A, B or b_i . To obtain the final results for linear and bi-linear models, we train the dictionaries and optimize A, B or b_i iteratively. For PK-NN, trainable weights are not only contained in dictionaries but also in the projected Koopman operator. We train them together

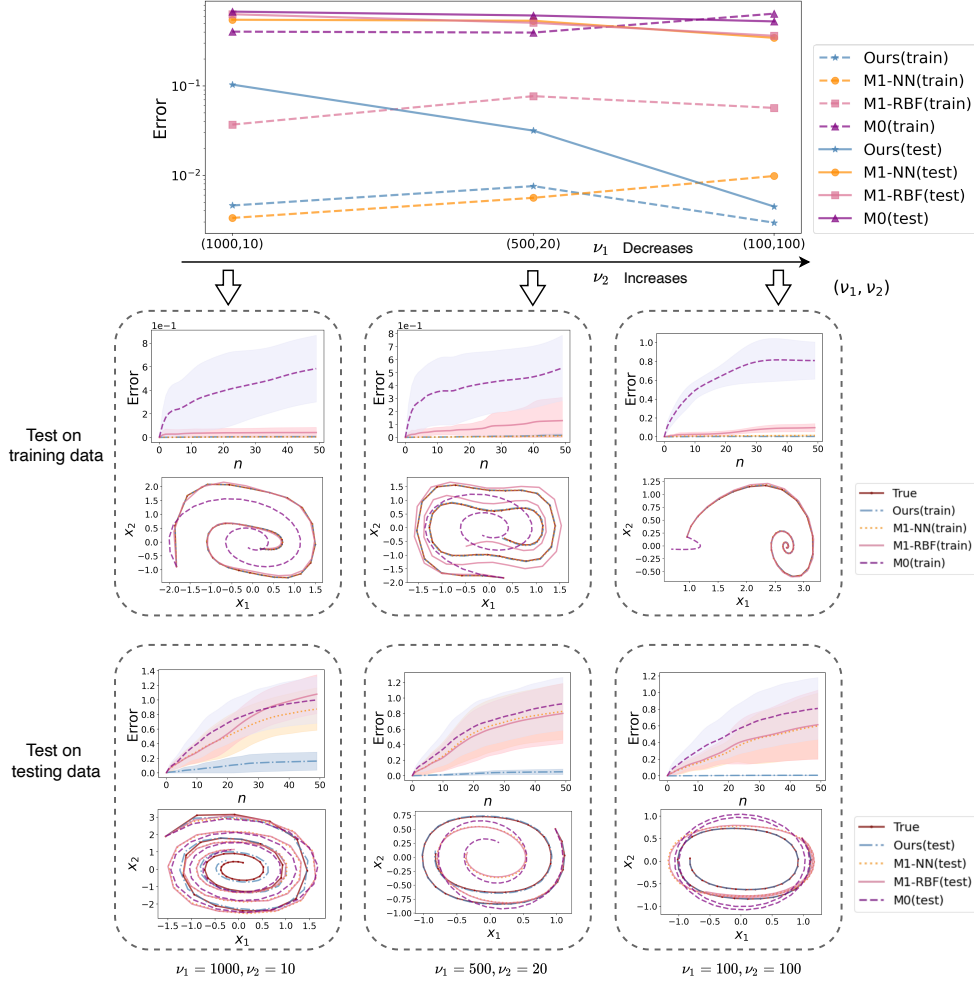


Fig. 2: Comparison on different (ν_1, ν_2) with $\nu_1 \nu_2 = 10000$. The topmost panel displays the prediction results for PK-NN and M1 on both training and testing data. The horizontal axis represents the values of (ν_1, ν_2) . In the bottom panels, we provide a detailed error analysis at varying time steps across various (ν_1, ν_2) configurations. We observe that PK-NN out-performs M1-NN, M1-RBF and M0 significantly when ν_2 increases, which results in fewer trajectories per parameter configuration.

to find an approximately optimal model. As shown in Figure 3, we show that PK-NN does not perform as well as linear and bi-linear model when $\mu = 0$ but improves upon them when $\mu = 1, 2, 3, 4$. This is expected since the system is closest to a non-linear/bi-linear system when $\mu = 0$, whereas it departs more significantly from a linear structure as μ increases. In Appendix D, we explain that PK-NN can still perform well when $\mu = 0$ using a perturbed initialization from a set of precise weights.

4.1.3. Improved accuracy for high-dimensional systems. We now apply PK-NN to the high-dimensional problem involving a variation of the FitzHugh-Nagumo partial differential equation subject to quasi-periodic forcing, which is men-

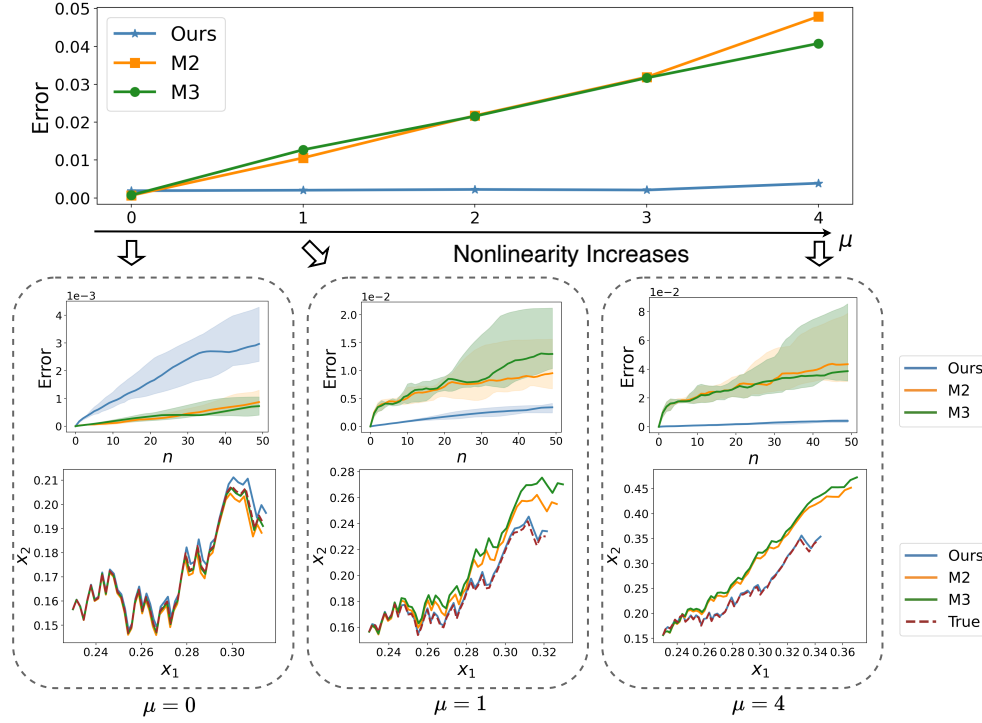


Fig. 3: A comparison of errors that occur as the non-linearity of variables \mathbf{u} and \mathbf{x} in the problem increases, with the variable μ acting the non-linearity coefficient. The topmost figure showcases the error analysis for PK-NN, linear model, and bi-linear model as the non-linearity coefficient μ is incremented. The bottom blocks illustrate a contrast between predicted trajectories of different methods and the exact solution, along with an error analysis at each time step for the corresponding μ configuration. PK-NN outperforms the other two structures when the non-linearity of the system increases.

tioned in [62]

$$(4.6) \quad \begin{aligned} \partial_t v &= \partial_{xx} v + v - v^3 - w + u(t)(e^{-(x-k_1)^2/2} + e^{-(x-k_2)^2/2} + e^{-(x-k_3)^2/2}), \\ \partial_t w &= \delta \partial_{xx} w + \epsilon(v - a_1 w - a_0). \end{aligned}$$

where $\delta = 4, \epsilon = 0.03, a_1 = 2, a_0 = -0.03, k_1 = -5, k_2 = 0, k_3 = 5$ on the domain $x \in (-10, 10)$ with Neumann boundary conditions. We adopt a finite difference method to discretize the spatial derivatives on a regular mesh consisting of 10 points. In this study, the state vector comprises two components: a 10-dimensional discretized activator complex \mathbf{v} and a 10-dimensional discretized inhibitor complex \mathbf{w} , resulting in a 20-dimensional state vector. The initial condition for the activator complex \mathbf{v} is given by $\sin(\frac{a\pi x}{10} + \frac{\pi}{2})$ where a is an integer randomly sampled from the range $(1, 20)$. The inhibitor complex \mathbf{w} is initialized to zero at all spatial points. The parameters $u \in \mathbb{R}$ along the trajectory are uniformly randomly generated in $(-1, 1)$. Training data are generated on 100 trajectories over 500 sampling time-steps and $\Delta t = 0.001$. We compare PK-NN with the method introduced in [62], which uses fixed radial basis

functions as the dictionaries on states and approximates the parametric Koopman operator as

$$(4.7) \quad K(\mathbf{u}) = \sum_{i=1}^{N_K} h_i(\mathbf{u}) K_i.$$

In this experiment, the parameter-dependent functions $h_i(\mathbf{u})$ are approximated by polynomials up to third order. We refer to this method by “M4-RBF” in the following figures. Furthermore, to observe the influence of the dictionaries on states, we introduce a modification called “M4-NN”, where the dictionaries are trainable, but the structure of $K(\mathbf{u})$ is the same as (4.7). In this experiment, the dictionary is designed as $(1, \mathbf{v}^T, \mathbf{w}^T, NN^T)^T$ where $\mathbf{v}, \mathbf{w} \in \mathbb{R}^{10}$ and NN is 10-dimensional trainable vector. NN utilizes two hidden layers with a width of 128, whereas NN_K employs one hidden layer with a width of 16.

In Figure 4(a), we show that trainable dictionaries lead to better prediction results than only using RBF, suggesting that adaptive dictionaries are effective for high-dimensional state spaces. Additionally, the performance of PK-NN aligns similarly to M4-NN. The reason may be the parameter \mathbf{u} in Equation (4.6) is one-dimensional, making the polynomial-based approximation of $K(\mathbf{u})$ sufficiently effective. To verify this hypothesis, we modify (4.6) to

$$(4.8) \quad \begin{aligned} \partial_t v &= \partial_{xx} v + v - v^3 - w + u_1(t)e^{-(x-k_1)^2/2} + u_2(t)e^{-(x-k_2)^2/2} + u_3(t)e^{-(x-k_3)^2/2}, \\ \partial_t w &= \delta \partial_{xx} w + \epsilon(v - a_1 w - a_0). \end{aligned}$$

with three parameters $\mathbf{u} = (u_1, u_2, u_3) \in \mathbb{R}^3$, while other settings remain unchanged. The number of trainable weights in K are kept approximately the same in both methods, whereas the dimensions of the state dictionary Ψ are identical. The dictionary retains a structure of $(1, \mathbf{v}^T, \mathbf{w}^T, NN^T)^T$. NN utilizes two hidden layers with a width of 128 and NN_K has two hidden layers with width 16. In Figure 4(b), we observe that PK-NN now performs better than the two baselines, consistent with our hypothesis. Expanding our investigation to encompass systems with higher dimensionality, Figure 4(c) shows an improvement in the performance of PK-NN as the spatial discretization range is broadened from 10 to 100 for (4.6) and PK-NN also outperforms other two methods. The results of the prediction on the original space, with $N_x = 10$ and $\dim \mathbf{u} = 1$, are presented in Figure 5. We can see that the predictions by PK-NN are more accurate than the other methods, M4-RBF and M4-NN. The results on $N_x = 10$, $\dim \mathbf{u} = 3$ and $N_x = 100$, $\dim \mathbf{u} = 1$ are shown in Appendix E. This demonstrates the effectiveness of our approach in handling high-dimensional systems.

4.2. Optimal control problems. As a final class of applications, we show that PK-NN can be used to solve optimal control problems from observational data without knowledge of the precise form of the dynamics that drive the control system. Furthermore, it can deal with strongly non-linear control systems, both in the state and the control.

We first apply our method to control the forced Korteweg-De Vries (KdV) equation ([40])

$$(4.9) \quad \frac{\partial \eta(t, x)}{\partial t} + \eta(t, x) \frac{\partial \eta(t, x)}{\partial x} + \frac{\partial^3 \eta(t, x)}{\partial x^3} = w(t, x),$$

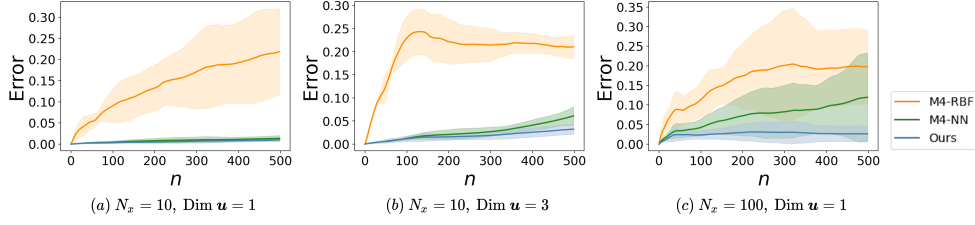


Fig. 4: Comparison of prediction errors computed from the three approaches on the FitzHugh-Nagumo PDE discretized on space \mathbf{x} , for varying dimensions of the parameter \mathbf{u} . We observe that as parameter dimension increases, PK-NN out-performs polynomial-based approximation schemes.

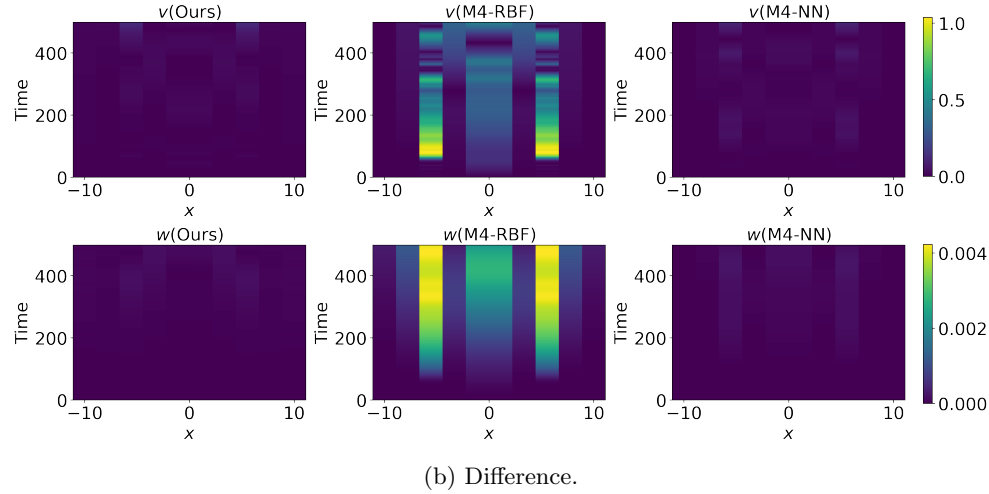
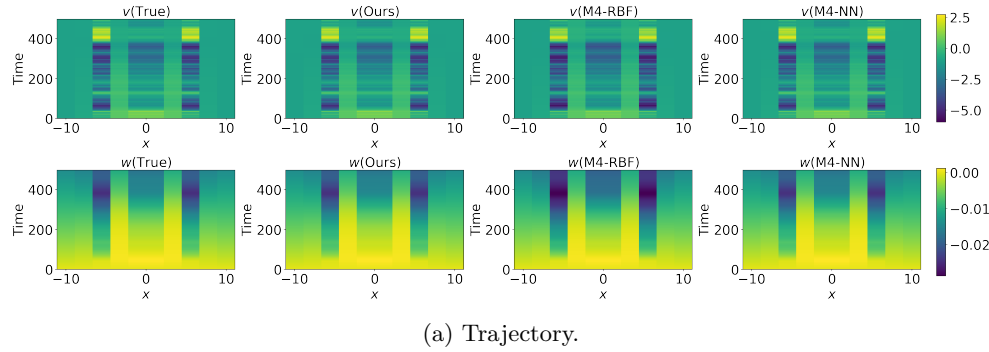


Fig. 5: (a): Prediction by PK-NN, M4-RBF and M4-NN on FHN system with $N_\psi = 10$ and $\text{dim } \mathbf{u} = 1$. (b): The absolute value of the difference between the forecasted outcomes and the ground truth.

where $w(t, x) = \sum_{i=1}^3 v_i(x) \sin(\pi u_i(t))$ is the forcing term. Control parameters at t_n are $\mathbf{u}_n = (u_{1,n}, u_{2,n}, u_{3,n})^T \in [-1, 1]^3$. The functions $v_i(x) = e^{-25(x-c_i)^2}$ are fixed spatial profiles with $c_1 = -\frac{\pi}{2}$, $c_2 = 0$ and $c_3 = \frac{\pi}{2}$ [31]. We consider periodic boundary conditions on the spatial variable $x \in [-\pi, \pi]$ and we discretize with a spatial mesh of 128 points, and the time step is $\Delta t = 0.01$. This induces a state-space $\boldsymbol{\eta}_n = (\eta_1(t_n), \eta_2(t_n), \dots, \eta_{128}(t_n))^T$ where $\eta_i(t_n)$ is the value of $\eta(t_n, x_i)$ at time t_n and x_i is the i^{th} spatial grid point.

We consider a tracking problem involving one of the following two observables: the “mass” $\int_X \eta(t, x) dx$ and the “momentum” $\int_X \eta^2(t, x) dx$. Given a reference trajectory (of either mass or momentum) $\{r_n\}$, the tracking problem refers to a Bolza problem (3.8) with $\Phi \equiv 0$ and $L_n(m, \mathbf{u}) = |m - r_n|^2$. Training data are generated from 1000 trajectories of length 200 samples. The initial conditions are a convex combination of three fixed spatial profiles and written as $\eta(0, x) = b_1 e^{-(x-\frac{\pi}{2})^2} + b_2 (-\sin(\frac{x}{2}))^2 + b_3 e^{-(x+\frac{\pi}{2})^2}$ with $b_i > 0$ and $\sum_{i=1}^3 b_i = 1$, b_i ’s are randomly sampled in $(0, 1)$ with uniform distribution. The training controls $u_i(t)$ are uniformly randomly generated in $[-1, 1]$. We design a common dictionary for the two tracking problems of the form $\boldsymbol{\Psi}(\boldsymbol{\eta}) = (1, \int_X \eta(t, x) dx, \int_X \eta^2(t, x) dx, NN(\boldsymbol{\eta}))^T$ with 3 trainable elements so that the resulting in the dimension of $\boldsymbol{\Psi}$ is 6. The NN is a residual network with two hidden layers having width 16 and NN_K has two hidden layers with a width of 36. The observable matrix B in (3.8) is the row vector $(0, 1, 0, 0, 0, 0)$ for mass tracking, while $B = (0, 0, 1, 0, 0, 0)$ for momentum tracking.

Instead of computing an optimal control using non-linear programming, we compute $\{\hat{\mathbf{u}}_n\}_{n=0}^{N-1}$ successively in time by solving (3.8) with model predictive control (MPC) [19]. We substitute the currently computed control into (4.9), which is integrated with RK23 [5] to get the next predicted state $\boldsymbol{\eta}_{n+1}$. This map is denoted by \mathbf{f} . The predicted state is the initial value at the next MPC step. In each MPC step, the parametric Koopman dynamics is used to solve for control inputs over a specified time horizon τ by minimizing the cost function [31]. Concretely, to obtain $\hat{\mathbf{u}}_n$ we solve the optimization problem

$$\begin{aligned}
 (4.10) \quad & \min_{\{\tilde{\mathbf{u}}_i\}_{i=n}^{n+\tau-1}} J = \sum_{i=n}^{n+\tau-1} (\|r_{i+1} - m_{i+1}\|^2 + \lambda \|\tilde{\mathbf{u}}_i\|^2) \\
 & \text{s.t. } m_{i+1} = B \prod_{j=0}^{i-n} K(\tilde{\mathbf{u}}_{n+j}) \boldsymbol{\Psi}(\hat{\boldsymbol{\eta}}_n), \quad i = n, \dots, n + \tau - 1, \\
 & \hat{\boldsymbol{\eta}}_n = \mathbf{f}(\hat{\boldsymbol{\eta}}_{n-1}, \hat{\mathbf{u}}_{n-1}), \quad \hat{\boldsymbol{\eta}}_0 = \boldsymbol{\eta}_0, \\
 & -1 \leq u_{k,n} \leq 1, \quad k = 1, 2, 3,
 \end{aligned}$$

giving $\{\tilde{\mathbf{u}}_i\}_{i=n}^{n+\tau-1}$, and then set $\hat{\mathbf{u}}_n = \tilde{\mathbf{u}}_n$. We iterate this for $n = 0, 1, \dots, N_T$ where N_T is the number of all the time steps in the control problem. Here, $\lambda \geq 0$ is a regularization coefficient.

In experiments, we compare three approaches: PK-NN, M2 (4.4) and M3 (4.5). All approaches utilize trainable state dictionaries with identical structures. The starting values of the tracking are computed by the state $\boldsymbol{\eta}(t_0) = 0.2$, then we get $m_0^{(\text{mass})} = 1.27$ and $m_0^{(\text{momentum})} = 0.25$. Our objective involves tracing the mass or momentum reference trajectories

$$r_n^{(\text{mass})} = \begin{cases} 1.90, & \text{for } n \leq 500 \\ 3.16, & \text{for } n > 500 \end{cases}, \quad r_n^{(\text{momentum})} = \begin{cases} 0.57, & \text{for } n \leq 500 \\ 1.58, & \text{for } n > 500 \end{cases}.$$

Before discussing how to solve this control problem, we show the predictions of mass and momentum in [Appendix G](#). PK-NN outperforms both M2 and M3 models on the forward prediction, providing a foundation for solving control problems. Now we shift our attention back to addressing the control problems. In [Figure 6](#), we present the tracking results for mass (a) and momentum (b) with the MPC horizon τ set to 10. When $\lambda = 0.005$, PK-NN exhibits better tracking capabilities than the other two methods, attributed to its ability to capture the inherent non-linearity present in [\(4.9\)](#). Furthermore, when considering mass tracking under $\lambda = 0$, [\(4.9\)](#) admits an explicit optimal control solution $u_{i,n} = \frac{1}{2}$ for $0 \leq n \leq 59$ and $500 \leq n \leq 619$ while $u_{i,n} = 0$ otherwise. This follows directly from integrating [\(4.9\)](#) over the spatial domain. The evolution of mass under this optimal control is labelled as “KdV” in figure (a) of [Figure 6](#). In the case of linear and bi-linear models, the absence of regularization in optimization leads to failure of mass tracking since the optimal control takes on the values ± 1 , i.e. on boundaries of the control set. Over this switching range, the control function $w(t, \cdot)$ cannot be well approximated by a linear function. Similarly, for momentum tracking ([Figure 6\(b\)](#)), PK-NN outperforms the other two methods, which struggle to track the reference.

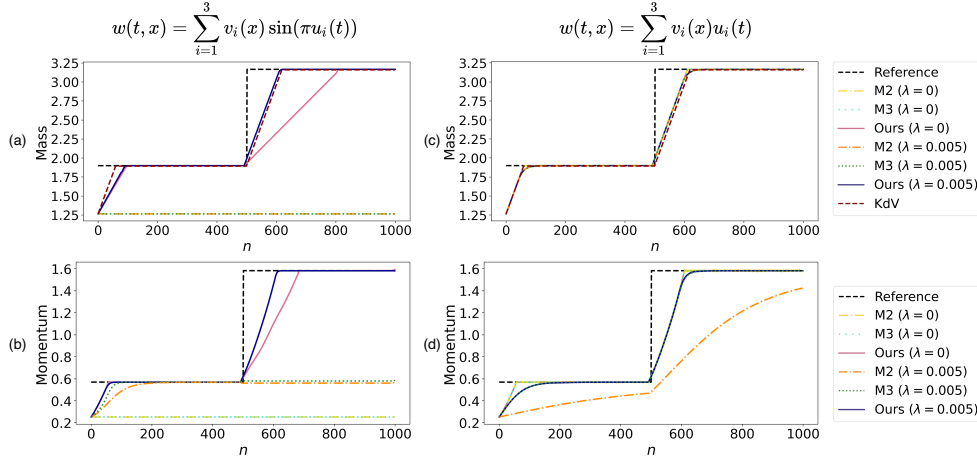


Fig. 6: Tracking results for KdV equation utilizing a piece-wise constant reference trajectory. Subfigures (a)-(b) illustrate tracking performance for mass and momentum observables under $w(t, x) = \sum_{i=1}^3 v_i(x) \sin(\pi u_i(t))$; Subfigures (c)-(d) present the same tracking comparison when $w(t, x) = \sum_{i=1}^3 v_i(x) u_i(t)$.

To confirm that the performance disparity is due to the non-linear dependence of the evolution equations on the control, we perform an ablation study by setting $w(t, x)$ in [\(4.9\)](#) to be $\sum_{i=1}^3 v_i(x) u_i(t)$, i.e. the forcing term depends linearly on the control. For $\lambda = 0$, a similar explicit optimal control can be derived ($u_{i,n} = 1$ when $0 \leq n \leq 59$ and $500 \leq n \leq 619$, and $u_{i,n} = 0$ otherwise). As expected, when the control system is linear, the tracking outcomes of these three approaches are similar when $\lambda = 0$, PK-NN and M3 out-perform M2 when $\lambda = 0.005$, as depicted in [Figure 6\(c\)](#) and (d). The optimization procedure employs the L-BFGS algorithm [\[36\]](#) using Python on a 3.20GHz Intel Xeon W-3245 with 125 GB of RAM. The average optimization times recorded are 5.82 seconds for the PK-NN model, 0.83 seconds for

M2, and 1.69 seconds for M3, indicating that, when using the same optimization software, the PK-NN model requires between three and seven times longer than the other two approaches. This observation shows that PK-NN demands substantially more computational resources than the other models. However, PK-NN achieves satisfactory optimization results and significantly improves control capabilities. The comparative analysis of computational costs is further elaborated in [Appendix I](#).

We have shown that PK-NN outperforms linear (M2) and bi-linear (M3) Koopman models on tracking problems due to the stronger non-linearity. To determine if PK-NN shows improvements over other non-linear methods, we add an experiment with standard nonlinear MPC (NMPC). We build a neural network \mathbf{f}_{NN} and train it on the same dataset to simulate the dynamics $\boldsymbol{\eta}_{n+1} = \mathbf{f}_{NN}(\boldsymbol{\eta}_n, \mathbf{u}_n)$. The NMPC approach first learns dynamics directly in the state space and then performs optimization to determine the controls, whereas the Koopman model focuses on learning within the observable space and controlling the observables directly. This results in NMPC being more inefficient when the state dimension is high. To demonstrate this, we consider problems with different spatial discretization resolutions N_x . We have discussed the results with $N_x = 128$ in our paper, and now we extend the experiments to $N_x = 64$ and $N_x = 256$. The neural network \mathbf{f}_{NN} uses a fully-connected architecture with ReLU as the activation function. Both the input and output are vectors of size N_x , which matches the dimension of $\boldsymbol{\eta}$. The parameter counts are determined by specifying a test error tolerance for forward prediction, measured by the mean absolute error in momentum prediction. The errors for different initial conditions are controlled to around 10^{-4} , and multi-step predictions over a horizon length equivalent to the MPC process are controlled to below 3×10^{-3} . We select the smallest network that can achieve this error tolerance. The complexity of the NMPC model significantly increases as N_x grows. [Table 2](#) outlines the model structures and parameter counts for PK-NN and NMPC across different N_x . Under these settings, we compare the tracking performance and computational cost of PK-NN and NMPC.

N_x	64	128	256
\mathbf{f}_{NN} Arch.	[512,512]	[768,768]	[1024,1024]
\mathbf{f}_{NN} Param. No.	330304	790400	1578240
PK-NN Arch. (Ψ & K)	[16, 16] & [36, 36]	[16, 16] & [36, 36]	[16, 16] & [36, 36]
PK-NN Param. No.	4205	5229	7277

Table 2: The comparison between PK-NN and NMPC model architectures and trainable parameter counts across different N_x .

Because \mathbf{f}_{NN} learns the dynamics of $\boldsymbol{\eta}$ not in the observable space, differing from

the Koopman model's setup, the tracking problem becomes

$$\begin{aligned}
 (4.11) \quad \min_{\{\tilde{\mathbf{u}}_i\}_{i=n}^{n+\tau-1}} \quad & J = \sum_{i=n}^{n+\tau-1} (\|r_{i+1} - m_{i+1}\|^2 + \lambda \|\tilde{\mathbf{u}}_i\|^2) \\
 \text{s.t.} \quad & m_{i+1} = \mathbf{g}(\tilde{\boldsymbol{\eta}}_{i+1}), \\
 & \tilde{\boldsymbol{\eta}}_{i+1} = \mathbf{f}_{NN}(\tilde{\boldsymbol{\eta}}_i, \tilde{\mathbf{u}}_i), \quad \tilde{\boldsymbol{\eta}}_n = \hat{\boldsymbol{\eta}}_n, \quad i = n, \dots, n + \tau - 1, \\
 & \hat{\boldsymbol{\eta}}_n = \mathbf{f}(\hat{\boldsymbol{\eta}}_{n-1}, \hat{\mathbf{u}}_{n-1}), \quad \hat{\boldsymbol{\eta}}_0 = \boldsymbol{\eta}_0, \\
 & -1 \leq u_{k,n} \leq 1, \quad k = 1, 2, 3,
 \end{aligned}$$

where \mathbf{g} is the observable function corresponding to mass or momentum depending on the problem. This optimization gives $\{\tilde{\mathbf{u}}_i\}_{i=n}^{n+\tau-1}$, and then sets $\hat{\mathbf{u}}_n = \tilde{\mathbf{u}}_n$. We iterate this for $n = 0, 1, \dots, N_T$ where N_T is the number of time steps in the control problem. In this experiment, we use NMPC to track the same observable “momentum” as PK-NN for the problem with non-linear forcing (sin) and $\lambda = 0.005$. The tracking results are shown in Figure 7(c), where both PK-NN and NMPC effectively track the reference trajectory but PK-NN performs faster and more accurately. We define the mean absolute error between the tracked trajectory and the reference as our evaluation metric. The comparison of tracking errors is illustrated in Figure 7(a), showing that PK-NN outperforms NMPC across different N_x , despite NMPC using a more complex neural network. Additionally, we compare the time consumed per epoch during the training of each model. As the number of trainable parameters increases, the training cost for the NMPC model rises sharply, as demonstrated in Figure 7(b). For the computational cost of solving the optimization problem during tracking, we compare the average, maximum, and minimum time per step for different N_x in Figure 7(d). When achieving similar tracking results, the average time cost for both training and tracking is higher for NMPC than for PK-NN. These results show that as the state dimension grows, both the training and tracking challenges for NMPC increase, but PK-NN is not significantly affected. However, when the state dimension is low, NMPC can also efficiently solve the problem. Although not explicitly indicated in the figures, it is evident that with lower dimensions, there is a trend of improvement in both tracking accuracy and training time.

We end with an analysis of the controllability of the learned parametric Koopman dynamics as discussed in subsection 3.4. Recall that a sufficient condition for controllability is for the matrix C (see (3.9)) to have full rank. When using a deep, fully connected network to approximate K , we can control the rank of C by setting N_K , the number of learned features (the width) of the penultimate layer. In the following, we repeat the previous experiments for $N_K = 37, 31, 13, 7$. After training, we uniformly randomly sample 2000 $\mathbf{u}_i \in U$ to compute the matrix C . The decay of the singular values of C is shown in Figure 8a. Note that the dimension of the dictionary is 6, and the components in the first row of the matrix $K(\mathbf{u})$ are constants. Hence, the rank condition in this setting reduces to $5 \times 6 = 30$. Only the case $N_K = 37$ satisfies the rank condition that guarantees controllability. We now solve the tracking problem under the three choices of N_K for $\lambda = 0.005$, and the results shown in Figure 8b and Figure 8c confirms that the tracking performance may improve with greater controllability. A detailed discussion can be found in Appendix C.

5. Conclusion. We propose and implement a data-driven methodology for creating approximate Koopman dynamics for parametric dynamical systems. The primary challenge with the Koopman operator lies in identifying the invariant subspace

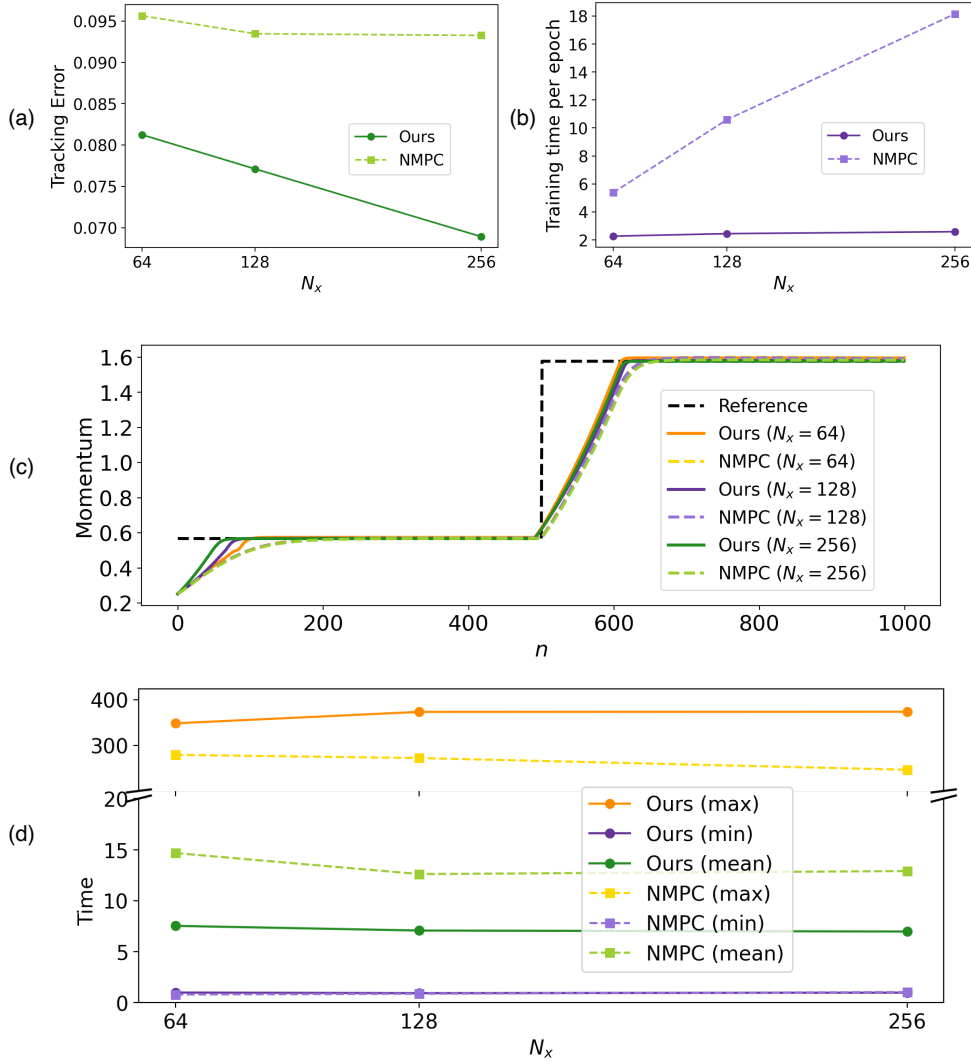


Fig. 7: Comparison between PK-NN and NMPC. (a) Tracking error results for both methods under different N_x . (b) Average time per epoch (in seconds) during model training for different N_x . (c) Tracking results for cases with varying N_x . (d) Time consumption per optimization step for solving tracking problems with different N_x , showing the average, maximum, and minimum values.

that is independent of parameters and approximating a projected Koopman operator that acts on this space. To address this, we use neural networks to parameterize both the parameter-dependent Koopman operator and the parameter-independent state dictionary that spans an invariant subspace. These are trained simultaneously using trajectory data, with a loss function designed to reflect the dynamics within the Koopman latent space.

In prediction tasks, PK-NN achieves improved performance over current methods,

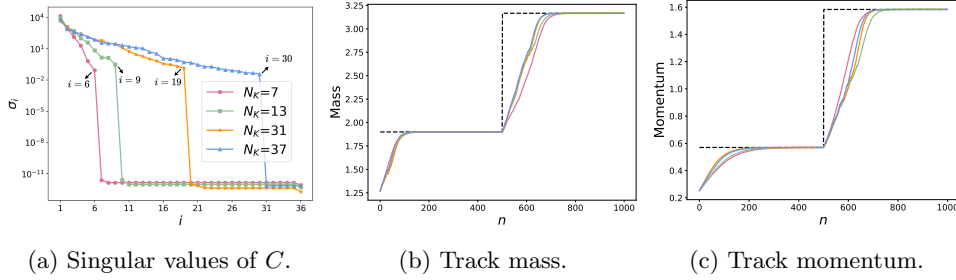


Fig. 8: Comparison on the controllability of PK-NN with $N_K = 7, 13, 37$.

including optimized DMD, EDMD with RBF dictionary and EDMD with dictionary learning. Our method performs well in handling highly non-linear problems, as evidenced by experiments with the Van der Pol Mathieu equations, surpassing linear and bilinear variants of the existing approach for parametric, or input-dependent, Koopman operator analysis. Additionally, PK-NN performs more effectively in scenarios involving high-dimensional states and parameters, outperforming existing Koopman structures generated by polynomial bases, with the FitzHugh-Nagumo (FhN) equation serving as a test case. In addition to prediction problems, in control applications our approach surpasses the performance of existing Koopman operator analysis with linear or bilinear control schemes, particularly in tracking observables in the Korteweg-de Vries (KdV) equation. This adaptability to high-dimensional and strongly non-linear problems makes our approach a suitable candidate for large-scale data-driven prediction and control applications.

Acknowledgements. The authors acknowledge discussions with MO Williams and Boyuan Liang at the initial stages of this work.

REFERENCES

- [1] F. ANDREUZZI, N. DEMO, AND G. ROZZA, *A dynamic mode decomposition extension for the forecasting of parametric dynamical systems*, SIAM Journal on Applied Dynamical Systems, 22 (2023), pp. 2432–2458.
- [2] D. ANGELI AND E. D. SONTAG, *Forward completeness, unboundedness observability, and their lyapunov characterizations*, Systems & Control Letters, 38 (1999), pp. 209–217.
- [3] H. ARBABI, M. KORDA, AND I. MEZIĆ, *A data-driven Koopman model predictive control framework for nonlinear partial differential equations*, in 2018 IEEE Conference on Decision and Control (CDC), IEEE, 2018, pp. 6409–6414.
- [4] M. J. BANKS, *Koopman Representations in Control*, PhD thesis, UC Santa Barbara, 2023. ProQuest ID: Banks.ucsb.0035D.16027. Merritt ID: ark:/13030/m5tj9f3g. Retrieved from <https://escholarship.org/uc/item/1gg8s7km>.
- [5] P. BOGACKI AND L. F. SHAMPINE, *A 3 (2) pair of runge-kutta formulas*, Applied Mathematics Letters, 2 (1989), pp. 321–325.
- [6] D. BRUDER, X. FU, R. B. GILLESPIE, C. D. REMY, AND R. VASUDEVAN, *Koopman-based control of a soft continuum manipulator under variable loading conditions*, IEEE Robotics and Automation Letters, 6 (2021), pp. 6852–6859.
- [7] D. BRUDER, X. FU, AND R. VASUDEVAN, *Advantages of bilinear Koopman realizations for the modeling and control of systems with unknown dynamics*, IEEE Robotics and Automation Letters, 6 (2021), pp. 4369–4376.
- [8] S. L. BRUNTON, M. BUDIĆIĆ, E. KAISER, AND J. N. KUTZ, *Modern Koopman theory for dynamical systems*, arXiv preprint arXiv:2102.12086, (2021).

- [9] M. BUDIŠIĆ, R. MOHR, AND I. MEZIĆ, *Applied Koopmanism*, Chaos: An Interdisciplinary Journal of Nonlinear Science, 22 (2012), p. 047510.
- [10] A. CHIUSO AND G. PILLONETTO, *System identification: A machine learning perspective*, Annual Review of Control, Robotics, and Autonomous Systems, 2 (2019), pp. 281–304.
- [11] W.-L. CHOW, *Über systeme von linearen partiellen differentialgleichungen erster ordnung*, Mathematische Annalen, 117 (1940), pp. 98–105.
- [12] V. CIBULKA, M. KORDA, AND T. HANIŠ, *Dictionary-free Koopman model predictive control with nonlinear input transformation*, arXiv preprint arXiv:2212.13828, (2022).
- [13] N. B. ERICHSON, M. MUEHLEBACH, AND M. W. MAHONEY, *Physics-informed autoencoders for lyapunov-stable fluid flow prediction*, arXiv preprint arXiv:1905.10866, (2019).
- [14] C. FOLKESTAD AND J. W. BURDICK, *Koopman NMPC: Koopman-based learning and nonlinear model predictive control of control-affine systems*, in 2021 IEEE International Conference on Robotics and Automation (ICRA), IEEE, 2021, pp. 7350–7356.
- [15] C. FOLKESTAD, D. PASTOR, I. MEZIC, R. MOHR, M. FONOVEROVA, AND J. BURDICK, *Extended dynamic mode decomposition with learned Koopman eigenfunctions for prediction and control*, in 2020 american control conference (acc), IEEE, 2020, pp. 3906–3913.
- [16] X. GLOROT AND Y. BENGIO, *Understanding the difficulty of training deep feedforward neural networks*, in Proceedings of the thirteenth international conference on artificial intelligence and statistics, JMLR Workshop and Conference Proceedings, 2010, pp. 249–256.
- [17] E. GONZALEZ, M. ABUDIA, M. JURY, R. KAMALAPURKAR, AND J. A. ROSENFELD, *Anti-koopmanism*, arXiv preprint arXiv:2106.00106, (2021).
- [18] D. GOSWAMI AND D. A. PALEY, *Global bilinearization and controllability of control-affine nonlinear systems: A Koopman spectral approach*, in 2017 IEEE 56th Annual Conference on Decision and Control (CDC), IEEE, 2017, pp. 6107–6112.
- [19] L. GRÜNE, J. PANNEK, L. GRÜNE, AND J. PANNEK, *Nonlinear model predictive control*, Springer, 2017.
- [20] Y. GUO, M. KORDA, I. G. KEVREKIDIS, AND Q. LI, *Code Repository for Learning Parametric Koopman Decompositions*, <https://github.com/GUOYUE-Cynthia/Learning-Parametric-Koopman-Decompositions>.
- [21] D. A. HAGGERTY, M. J. BANKS, P. C. CURTIS, I. MEZIĆ, AND E. W. HAWKES, *Modeling, reduction, and control of a helically actuated inertial soft robotic arm via the Koopman operator*, arXiv preprint arXiv:2011.07939, (2020).
- [22] M. HASELI AND J. CORTÉS, *Temporal forward-backward consistency, not residual error, measures the prediction accuracy of extended dynamic mode decomposition*, IEEE Control Systems Letters, 7 (2022), pp. 649–654.
- [23] M. HASELI AND J. CORTÉS, *Modeling Nonlinear Control Systems via Koopman Control Family: Universal Forms and Subspace Invariance Proximity*, arXiv preprint arXiv:2307.15368, (2023).
- [24] P. HÉAS AND C. HERZET, *Low-rank dynamic mode decomposition: An exact and tractable solution*, Journal of Nonlinear Science, 32 (2022), p. 8.
- [25] E. HILLE AND R. S. PHILLIPS, *Functional analysis and semi-groups*, vol. 31, American Mathematical Soc., 1996.
- [26] Q. A. HUHN, M. E. TANO, J. C. RAGUSA, AND Y. CHOI, *Parametric dynamic mode decomposition for reduced order modeling*, Journal of Computational Physics, 475 (2023), p. 111852.
- [27] H. JIANLIANG, W. TENG, AND C. SHUHUI, *Nonlinear dynamic analysis of a van der pol-mathieu equation with external excitation*, Chinese Journal of Theoretical and Applied Mechanics, 53 (2021), pp. 496–510.
- [28] E. KAISER, J. N. KUTZ, AND S. L. BRUNTON, *Data-driven discovery of Koopman eigenfunctions for control*, arXiv preprint arXiv:1707.01146, (2017).
- [29] D. P. KINGMA AND J. BA, *Adam: A method for stochastic optimization*, arXiv preprint arXiv:1412.6980, (2014).
- [30] B. O. KOOPMAN, *Hamiltonian systems and transformation in hilbert space*, Proceedings of the national academy of sciences of the united states of america, 17 (1931), p. 315.
- [31] M. KORDA AND I. MEZIĆ, *Linear predictors for nonlinear dynamical systems: Koopman operator meets model predictive control*, Automatica, 93 (2018), pp. 149–160.
- [32] M. KORDA AND I. MEZIĆ, *On convergence of extended dynamic mode decomposition to the Koopman operator*, Journal of Nonlinear Science, 28 (2018), pp. 687–710.
- [33] M. KORDA AND I. MEZIĆ, *Optimal construction of Koopman eigenfunctions for prediction and control*, IEEE Transactions on Automatic Control, 65 (2020), pp. 5114–5129.
- [34] Q. LI, F. DIETRICH, E. M. BOLLE, AND I. G. KEVREKIDIS, *Extended dynamic mode decomposition with dictionary learning: A data-driven adaptive spectral decomposition of the Koopman operator*, Chaos: An Interdisciplinary Journal of Nonlinear Science, 27 (2017),

- p. 103111.
- [35] K. K. LIN AND F. LU, *Data-driven model reduction, Wiener projections, and the Koopman-Mori-Zwanzig formalism*, Journal of Computational Physics, 424 (2021), p. 109864.
 - [36] D. C. LIU AND J. NOCEDAL, *On the limited memory bfgs method for large scale optimization*, Mathematical programming, 45 (1989), pp. 503–528.
 - [37] L. LJUNG, C. ANDERSSON, K. TIELS, AND T. B. SCHÖN, *Deep learning and system identification*, IFAC-PapersOnLine, 53 (2020), pp. 1175–1181.
 - [38] B. LUSCH, J. N. KUTZ, AND S. L. BRUNTON, *Deep learning for universal linear embeddings of nonlinear dynamics*, Nature communications, 9 (2018), p. 4950.
 - [39] A. MAUROY, Y. SUSUKI, AND I. MEZIĆ, *Koopman operator in systems and control*, Springer, 2020.
 - [40] R. M. MIURA, *The korteweg-devries equation: a survey of results*, SIAM review, 18 (1976), pp. 412–459.
 - [41] A. NARASINGAM AND J. S.-I. KWON, *Application of Koopman operator for model-based control of fracture propagation and proppant transport in hydraulic fracturing operation*, Journal of Process Control, 91 (2020), pp. 25–36.
 - [42] S. E. OTTO AND C. W. ROWLEY, *Linearly recurrent autoencoder networks for learning dynamics*, SIAM Journal on Applied Dynamical Systems, 18 (2019), pp. 558–593.
 - [43] S. PAN AND K. DURAISAMY, *Physics-informed probabilistic learning of linear embeddings of nonlinear dynamics with guaranteed stability*, SIAM Journal on Applied Dynamical Systems, 19 (2020), pp. 480–509.
 - [44] N. PARMAR, H. REFAI, AND T. RUNOLFSSON, *A Survey on the Methods and Results of Data-Driven Koopman Analysis in the Visualization of Dynamical Systems*, IEEE Transactions on Big Data, (2020).
 - [45] S. PEITZ AND S. KLUS, *Koopman operator-based model reduction for switched-system control of PDEs*, Automatica, 106 (2019), pp. 184–191.
 - [46] S. PEITZ, S. E. OTTO, AND C. W. ROWLEY, *Data-driven model predictive control using interpolated Koopman generators*, SIAM Journal on Applied Dynamical Systems, 19 (2020), pp. 2162–2193.
 - [47] J. L. PROCTOR, S. L. BRUNTON, AND J. N. KUTZ, *Dynamic mode decomposition with control*, SIAM Journal on Applied Dynamical Systems, 15 (2016), pp. 142–161.
 - [48] J. L. PROCTOR, S. L. BRUNTON, AND J. N. KUTZ, *Generalizing Koopman theory to allow for inputs and control*, SIAM Journal on Applied Dynamical Systems, 17 (2018), pp. 909–930.
 - [49] P. RASHEVSKY, *About connecting two points of a completely nonholonomic space by admissible curve*, Uch. Zapiski Ped. Inst. Libknechta, 2 (1938), pp. 83–94.
 - [50] C. W. ROWLEY, I. MEZIĆ, S. BAGHERI, P. SCHLATTER, AND D. S. HENNINGSON, *Spectral analysis of nonlinear flows*, Journal of fluid mechanics, 641 (2009), pp. 115–127.
 - [51] P. J. SCHMID, *Dynamic mode decomposition of numerical and experimental data*, Journal of fluid mechanics, 656 (2010), pp. 5–28.
 - [52] H. SHI AND M. Q.-H. MENG, *Deep Koopman operator with control for nonlinear systems*, IEEE Robotics and Automation Letters, 7 (2022), pp. 7700–7707.
 - [53] R. K. SINGH AND J. S. MANHAS, *Composition operators on function spaces*, Elsevier, 1993.
 - [54] J.-J. E. SLOTTINE, W. LI, ET AL., *Applied nonlinear control*, vol. 199, Prentice hall Englewood Cliffs, NJ, 1991.
 - [55] S. H. SON, H.-K. CHOI, AND J. S.-I. KWON, *Application of offset-free Koopman-based model predictive control to a batch pulp digester*, AIChE Journal, 67 (2021), p. e17301.
 - [56] R. STRÄSSER, J. BERBERICH, AND F. ALLGÖWER, *Robust data-driven control for nonlinear systems using the Koopman operator*, arXiv preprint arXiv:2304.03519, (2023).
 - [57] S. SUN, L. FENG, H. S. CHAN, T. MILIČIĆ, T. VIDAKOVIĆ-KOCH, AND P. BENNER, *Parametric dynamic mode decomposition for nonlinear parametric dynamical systems*, arXiv preprint arXiv:2305.06197, (2023).
 - [58] A. SURANA, *Koopman operator based observer synthesis for control-affine nonlinear systems*, in 2016 IEEE 55th Conference on Decision and Control (CDC), IEEE, 2016, pp. 6492–6499.
 - [59] N. TAKEISHI, Y. KAWAHARA, AND T. YAIRI, *Learning koopman invariant subspaces for dynamic mode decomposition*, Advances in neural information processing systems, 30 (2017).
 - [60] D. N. TANYU, J. NING, T. FREUDENBERG, N. HEILENKÖTTER, A. RADEMACHER, U. IBEN, AND P. MAASS, *Deep learning methods for partial differential equations and related parameter identification problems*, arXiv preprint arXiv:2212.03130, (2022).
 - [61] J. H. TU, C. W. ROWLEY, D. M. LUCHTENBURG, S. L. BRUNTON, AND J. N. KUTZ, *On dynamic mode decomposition: Theory and applications*, Journal of Computational Dynamics, 1 (2014), pp. 391–421.
 - [62] M. O. WILLIAMS, M. S. HEMATI, S. T. DAWSON, I. G. KEVREKIDIS, AND C. W. ROWLEY,

- Extending data-driven Koopman analysis to actuated systems*, IFAC-PapersOnLine, 49 (2016), pp. 704–709.
- [63] M. O. WILLIAMS, I. G. KEVREKIDIS, AND C. W. ROWLEY, *A data-driven approximation of the Koopman operator: Extending dynamic mode decomposition*, Journal of Nonlinear Science, 25 (2015), pp. 1307–1346.
- [64] M. O. WILLIAMS, C. W. ROWLEY, AND I. G. KEVREKIDIS, *A kernel-based approach to data-driven Koopman spectral analysis*, arXiv preprint arXiv:1411.2260, (2014).
- [65] E. YEUNG, S. KUNDU, AND N. HODAS, *Learning deep neural network representations for Koopman operators of nonlinear dynamical systems*, in 2019 American Control Conference (ACC), IEEE, 2019, pp. 4832–4839.

Appendix A. Proof of Proposition 2.1.

Proof. For each \mathbf{u} , we suppose $\mathcal{K}(\mathbf{u})$ is the composition operator induced by $\mathbf{f}(\cdot, \mathbf{u})$. We consider $S \in \mathcal{S}$ such that $m(S) < \infty$, then the indicator function $\mathbf{1}_S \in L^2(X, m)$. If $\mathbf{x} \in \mathbf{f}^{-1}(\cdot, \mathbf{u})(S)$, we have $\mathbf{f}(\mathbf{x}, \mathbf{u}) \in S$ since $\mathbf{f}(\cdot, \mathbf{u})$ is non-singular. It is equivalent to $(\mathbf{1}_S \circ \mathbf{f}(\cdot, \mathbf{u}))(\mathbf{x}) = 1$, which induces $\mathcal{K}(\mathbf{u})\mathbf{1}_S(\mathbf{x}) = 1$. Thus, we have $\mathcal{K}(\mathbf{u})\mathbf{1}_S = \mathbf{1}_{\mathbf{f}^{-1}(\cdot, \mathbf{u})(S)}$. Then we have

$$\begin{aligned}
 m(\mathbf{f}^{-1}(\cdot, \mathbf{u})(S)) &= \int \mathbf{1}_{\mathbf{f}^{-1}(\cdot, \mathbf{u})(S)} dm \\
 &= \int \mathcal{K}(\mathbf{u})\mathbf{1}_S dm \\
 (A.1) \quad &= \int |\mathcal{K}(\mathbf{u})\mathbf{1}_S|^2 dm \\
 &= \|\mathcal{K}(\mathbf{u})\mathbf{1}_S\|^2 \\
 &\leq \|\mathcal{K}(\mathbf{u})\|^2 \|\mathbf{1}_S\|^2 \\
 &= \|\mathcal{K}(\mathbf{u})\|^2 m(S),
 \end{aligned}$$

where $\|\mathcal{K}\| = \sup_{\|\phi\|=1} \|\mathcal{K}\phi\|$. Let $b_{\mathbf{u}} = \|\mathcal{K}(\mathbf{u})\|^2$. Then we have $m(\mathbf{f}^{-1}(\cdot, \mathbf{u})(S)) \leq b_{\mathbf{u}}m(S)$.

Conversely, if we have $m(\mathbf{f}^{-1}(\cdot, \mathbf{u})(S)) \leq b_{\mathbf{u}}m(S)$, then $m\mathbf{f}^{-1}(\cdot, \mathbf{u}) \ll m$ (“ \ll ” means absolute continuity). The Radon-Nikodym derivative $h_{\mathbf{f}(\cdot, \mathbf{u})}$ of $m\mathbf{f}^{-1}(\cdot, \mathbf{u})$ with respect to m exists and $h_{\mathbf{f}(\cdot, \mathbf{u})} \leq b_{\mathbf{u}}$ almost everywhere. Let $\phi \in L^2(X, m)$ and then we have

$$\begin{aligned}
 (A.2) \quad \|\mathcal{K}(\mathbf{u})\phi\|^2 &= \int |\phi \circ \mathbf{f}(\cdot, \mathbf{u})|^2 dm = \int |\phi|^2 dm \mathbf{f}^{-1}(\cdot, \mathbf{u}) = \int |\phi|^2 h_{\mathbf{f}(\cdot, \mathbf{u})} dm \leq b_{\mathbf{u}}\|\phi\|^2.
 \end{aligned}$$

This shows that $\mathcal{K}(\mathbf{u})$ is a bounded (and continuous) operator on $L^2(X, m)$. \square

Appendix B. Proof of Proposition 3.1. In this section, we prove Proposition 3.1. The following Lemma B.1 and Lemma B.2 are necessary for our discussion.

LEMMA B.1. *Let X be a finite measurable space with measure m . If $(e_i)_{i=1}^\infty$ form an orthonormal basis of space $C_b(X)$. Define $P_N g = \operatorname{argmin}_{\tilde{g} \in \operatorname{span}((e_i)_{i=1}^\infty)} \|\tilde{g} - g\|$, then P_N converge strongly to the identity operator I .*

Proof. Let $\phi = \sum_{i=1}^\infty c_i e_i$ with $\|\phi\| = 1$. Then by Parseval's identity $\sum_{i=1}^\infty |c_i|^2 = 1$ and

$$(B.1) \quad \|P_N \phi - \phi\|^2 = \left\| \sum_{i=N+1}^\infty c_i e_i \right\|^2 = \sum_{i=N+1}^\infty |c_i|^2 \rightarrow 0, \quad \text{as } N \rightarrow \infty. \quad \square$$

LEMMA B.2. *Let X be a finite measurable space with measure m . Given an observable function $\phi \in C_b(X)$. Assume that $\mathbf{f}(\mathbf{x}, \cdot) : U \rightarrow X$ is continuous for almost all $\mathbf{x} \in X$. If (2.3) holds, then $\mathcal{K}(\cdot)\phi : U \rightarrow C_b(X)$ is continuous on U with respect to L^2 norm, in the sense that $\lim_{\mathbf{u}_n \rightarrow \mathbf{u}} \|\mathcal{K}(\mathbf{u}_n)\phi - \mathcal{K}(\mathbf{u})\phi\| = 0$.*

Proof. Since $\mathbf{f}(\mathbf{x}, \mathbf{u}_n) \rightarrow \mathbf{f}(\mathbf{x}, \mathbf{u})$ as $\mathbf{u}_n \rightarrow \mathbf{u}$ almost everywhere $\mathbf{x} \in X$ and $\phi(\mathbf{x})$ is a continuous function, we have

$$(B.2) \quad \lim_{\mathbf{u}_n \rightarrow \mathbf{u}} |\phi \circ \mathbf{f}(\mathbf{x}, \mathbf{u}_n) - \phi \circ \mathbf{f}(\mathbf{x}, \mathbf{u})|^2 = 0$$

almost everywhere on X . Since $|\phi(\mathbf{x})| \leq M$ on X for some $M \in [0, \infty)$, we have $|\phi \circ \mathbf{f}(\mathbf{x}, \mathbf{u}_n) - \phi \circ \mathbf{f}(\mathbf{x}, \mathbf{u})|^2 \leq 4M^2$. By the dominated convergence theorem,

$$\begin{aligned}
 \lim_{\mathbf{u}_n \rightarrow \mathbf{u}} \|\mathcal{K}(\mathbf{u}_n)\phi - \mathcal{K}(\mathbf{u})\phi\|^2 &= \lim_{\mathbf{u}_n \rightarrow \mathbf{u}} \int_X |\mathcal{K}(\mathbf{u}_n)\phi(\mathbf{x}) - \mathcal{K}(\mathbf{u})\phi(\mathbf{x})|^2 m(d\mathbf{x}) \\
 &= \lim_{\mathbf{u}_n \rightarrow \mathbf{u}} \int_X |\phi \circ \mathbf{f}(\mathbf{x}, \mathbf{u}_n) - \phi \circ \mathbf{f}(\mathbf{x}, \mathbf{u})|^2 m(d\mathbf{x}) \\
 &= \int_X \lim_{\mathbf{u}_n \rightarrow \mathbf{u}} |\phi \circ \mathbf{f}(\mathbf{x}, \mathbf{u}_n) - \phi \circ \mathbf{f}(\mathbf{x}, \mathbf{u})|^2 m(d\mathbf{x}) \\
 &= 0.
 \end{aligned}
 \tag{B.3}$$

Therefore, $\lim_{\mathbf{u}_n \rightarrow \mathbf{u}} \|\mathcal{K}(\mathbf{u}_n)\phi - \mathcal{K}(\mathbf{u})\phi\| = 0$. \square

In [Proposition B.3](#), we demonstrate that an inequality employed in the proof of [Proposition 3.1](#) is applicable to a finite set of parameters for given observables.

PROPOSITION B.3. *Let $U = \{\mathbf{u}_1, \mathbf{u}_2, \dots, \mathbf{u}_s\}$ be a finite set of parameters and assume that the observables of interest \mathbf{g} satisfy $g_j \in C_b(X)$. Then, for any $\varepsilon > 0$, there exists a positive integer $N_\psi > 0$, a dictionary $\Psi = \{\psi_1, \dots, \psi_{N_\psi}\}$ with $\psi_i \in L^2(X, m)$, a set of vectors $\{\mathbf{a}_j \in \mathbb{R}^{N_\psi} : j = 1, \dots, N_y\}$, such that $g_j = \mathbf{a}_j^T \Psi$ and for all $\mathbf{u} \in U$, we have $\|\mathcal{K}(\mathbf{u})g_j - P_{N_\psi} \mathcal{K}(\mathbf{u})g_j\| \leq \varepsilon$, where $P_{N_\psi} g = \operatorname{argmin}_{\tilde{g} \in \operatorname{span}(\Psi_{N_\psi})} \|\tilde{g} - g\|$.*

Proof. Let $\psi_j = g_j, j = 1, \dots, N_y$ and this can ensure the existence of \mathbf{a}_j . Let $(\psi_i)_{i=1}^\infty$ be a sequence of functions in $C_b(X)$ such that $\operatorname{span}((\psi_i)_{i=1}^\infty)$ is dense in $C_b(X)$. The dictionary $\Psi_N = (\psi_1(\mathbf{x}), \psi_2(\mathbf{x}), \dots, \psi_N(\mathbf{x}))^T$ consists of the first N elements of $(\psi_i)_{i=1}^\infty$. Then we can compute an orthonormal basis $(e_i)_{i=1}^N$ of $\operatorname{span}(\Psi_N)$ by Gram-Schmidt process and note $(e_i)_{i=1}^\infty$ as an orthonormal basis of $C_b(X)$ space. Thus, $\operatorname{span}(\Psi_N) = \operatorname{span}((e_i)_{i=1}^N)$ and $P_N g = \operatorname{argmin}_{\tilde{g} \in \operatorname{span}((e_i)_{i=1}^N)} \|\tilde{g} - g\|$ by definition.

For each $\mathbf{u}_i \in U$, we have $\mathbf{x}_{n+1} = \mathbf{f}(\mathbf{x}_n, \mathbf{u}_i)$ and $g_j(\mathbf{x}_{n+1}) = \mathcal{K}(\mathbf{u}_i)g_j(\mathbf{x}_n)$. By [Lemma B.1](#), for any $\varepsilon_i > 0$, there exists $N_{i,j}^* \in \mathbb{N}^+$ such that $N_{i,j} \geq N_{i,j}^*$ implies

$$\frac{\|\mathcal{K}(\mathbf{u}_i)g_j - P_{N_{i,j}} \mathcal{K}(\mathbf{u}_i)g_j\|}{\|\mathcal{K}(\mathbf{u}_i)g_j\|} = \left\| \frac{\mathcal{K}(\mathbf{u}_i)g_j}{\|\mathcal{K}(\mathbf{u}_i)g_j\|} - P_{N_{i,j}} \frac{\mathcal{K}(\mathbf{u}_i)g_j}{\|\mathcal{K}(\mathbf{u}_i)g_j\|} \right\| \leq \varepsilon_i
 \tag{B.4}$$

for each j . Let $N_i = \max\{N_{i,j}^* : j=1, \dots, N_y\}$. Then we note that

$$\|\mathcal{K}(\mathbf{u}_i)g_j - P_{N_i} \mathcal{K}(\mathbf{u}_i)g_j\| = \frac{\|\mathcal{K}(\mathbf{u}_i)g_j - P_{N_i} \mathcal{K}(\mathbf{u}_i)g_j\|}{\|\mathcal{K}(\mathbf{u}_i)g_j\|} \|\mathcal{K}(\mathbf{u}_i)g_j\| \leq \varepsilon_i \sqrt{b_{\mathbf{u}_i}} \|g_j\|.
 \tag{B.5}$$

Given $\varepsilon > 0$, we set $\varepsilon_i = \frac{\varepsilon}{\sqrt{b_{\mathbf{u}_i}} \max\{\|g_j\|\}}$ and $b_{\mathbf{u}_i}$ is the coefficient discussed in [Proposition 2.1](#). Then for each \mathbf{u}_i , there exists a corresponding N_i such that the inequality [\(B.5\)](#) holds. Define $N_\psi = \max\{N_1, N_2, \dots, N_n\}$, then

$$\|\mathcal{K}(\mathbf{u}_i)g_j - P_{N_\psi} \mathcal{K}(\mathbf{u}_i)g_j\| \leq \varepsilon
 \tag{B.6}$$

holds for all $\mathbf{u}_i \in U_n$ and all the given g_j 's. \square

Now we have the **proof of Proposition 3.1**.

Proof. Step 1: By [Lemma B.2](#), for each given observable $g_j, \mathcal{K}(\cdot)g_j : U \rightarrow C_b(X)$ is uniformly continuous on compact set U . We know that for any $\varepsilon' > 0, \exists \delta_j > 0$ such that $\|\mathcal{K}(\mathbf{v})g_j - \mathcal{K}(\mathbf{u})g_j\| \leq \varepsilon'$ for any $\|\mathbf{v} - \mathbf{u}\| \leq \delta_j$. Let $\delta = \min\{\delta_j\}$. We

introduce the notion of a localized neighbourhood around each point \mathbf{v}_i in the set U . This neighbourhood is formally defined as

$$(B.7) \quad B_i = \{\mathbf{u} \in U : \|\mathbf{v}_i - \mathbf{u}\| \leq \delta, \mathbf{v}_i \in U\},$$

where δ is a predetermined positive radius. Given the collection $\{B_i\}$, it suffices to form an open cover for U . By the compactness of U , we can assert the existence of a finite subcover, denoted as $\{B_1, B_2, \dots, B_{n^*}\}$, which is sufficient to entirely cover the set U .

For each g_j , we denote $A_{i,j} = \mathcal{K}(B_i)g_j$ as the image of B_i by $\mathcal{K}(\cdot)g_j$. Then we have $\|\mathcal{K}(\mathbf{v}_i)g_j - g'\| \leq \varepsilon'$ for any $g' \in A_{i,j}$ and the collection $\{A_{1,j}, A_{2,j}, \dots, A_{n^*,j}\}$ can cover $A_j = \mathcal{K}(U)g_j$. Naturally, for any $\mathbf{u} \in B_i$, we have $\|\mathbf{v}_i - \mathbf{u}\| \leq \delta$ and

$$(B.8) \quad \|\mathcal{K}(\mathbf{v}_i)g_j - \mathcal{K}(\mathbf{u})g_j\| \leq \varepsilon'$$

for all given g_j 's.

Step 2: Let us consider how to get the dimension N_ψ of the dictionary Ψ by [Proposition B.3](#). For any $\varepsilon' > 0$, N_ψ can be determined by $\{\mathbf{v}_i\}_{i=1}^{n^*}$ which are the centers of $\{B_i\}_{i=1}^{n^*}$, such that

$$(B.9) \quad \|\mathcal{K}(\mathbf{v}_i)g_j - P_{N_\psi}\mathcal{K}(\mathbf{v}_i)g_j\| \leq \varepsilon'$$

for any $\mathbf{v}_i \in \{\mathbf{v}_i\}_{i=1}^{n^*}$ and all given g_j 's.

Step 3: Follow step 1, for any $\mathbf{u} \in B_i$ and all given g_j 's, the corresponding P_{N_ψ} can give

$$(B.10) \quad \begin{aligned} \|P_{N_\psi}\mathcal{K}(\mathbf{v}_i)g_j - P_{N_\psi}\mathcal{K}(\mathbf{u})g_j\| &= \|P_{N_\psi}(\mathcal{K}(\mathbf{v}_i)g_j - \mathcal{K}(\mathbf{u})g_j)\| \\ &\leq \|P_{N_\psi}\| \|\mathcal{K}(\mathbf{v}_i)g_j - \mathcal{K}(\mathbf{u})g_j\| \\ &\leq \varepsilon' \end{aligned}$$

since $\|P_{N_\psi}\| \leq 1$.

Step 4: We consider the analysis for any $\mathbf{u} \in U$, then \mathbf{u} must belong to at least one of the neighbourhoods $\{B_i\}_{i=1}^{n^*}$. If $\mathbf{u} \in B_i$, we consider [\(B.9\)](#), [\(B.8\)](#) and [\(B.10\)](#) and obtain

$$(B.11) \quad \begin{aligned} &\|\mathcal{K}(\mathbf{u})g_j - P_{N_\psi}\mathcal{K}(\mathbf{u})g_j\| \\ &\leq \|\mathcal{K}(\mathbf{u})g_j - \mathcal{K}(\mathbf{v}_i)g_j\| + \|\mathcal{K}(\mathbf{v}_i)g_j - P_{N_\psi}\mathcal{K}(\mathbf{v}_i)g_j\| + \|P_{N_\psi}\mathcal{K}(\mathbf{v}_i)g_j - P_{N_\psi}\mathcal{K}(\mathbf{u})g_j\| \\ &\leq \varepsilon, \end{aligned}$$

when we set $\varepsilon' = \frac{\varepsilon}{3}$.

Step 5: Notice that for any $\mathbf{u} \in U$, there exists a matrix $K(\mathbf{u}) \in \mathbb{R}^{N_\psi \times N_\psi}$ such that

$$(B.12) \quad P_{N_\psi}\mathcal{K}(\mathbf{u})g_j = \mathbf{a}_j^T K(\mathbf{u})\Psi,$$

where Ψ is defined as discussed in the proof of [Proposition B.3](#). Since $\mathcal{K}(\cdot)g_j : U \rightarrow C_b(X)$ is continuous on U , then $\mathbf{a}_j^T K(\cdot)\Psi : U \rightarrow C_b(X)$ is continuous on U for $j = 1, 2, \dots, N_y$. Thus, the entries in K are continuous on U . Then we note that $K : U \rightarrow \mathbb{R}^{N_\psi \times N_\psi}$ is a continuous function with respect to Frobenius norm and

$$(B.13) \quad \|\mathcal{K}(\mathbf{u})g_j - \mathbf{a}_j^T K(\mathbf{u})\Psi\| = \|\mathcal{K}(\mathbf{u})g_j - P_{N_\psi}\mathcal{K}(\mathbf{u})g_j\| \leq \varepsilon. \quad \square$$

Appendix C. Neural network structure of $K(u)$.

In this section, we explore the relationship between the number of nodes in the last hidden layer of neural network structure for $K(u)$ and the rank of matrix C . The structure of $K(u)$ is illustrated in Figure 9 and the matrix C is discussed in subsection 3.3. We explain this relationship by focusing on the KdV case detailed in subsection 4.2. In our setting, $d = N_\psi$. The output layer in our neural network configuration for $K(u)$ is a dense layer that includes a bias term. Therefore, if $N_{(\text{last hidden})}$ is the number of nodes in the last hidden layer, N_K should be $N_{(\text{last hidden})} + 1$. We can regard the flattened matrix $K(u)$ as the vector obtained prior to the “reshape” operation. Each element in this vector is computed by N_K basis functions. Consequently, the rank of matrix C is determined by $\min\{N_K, d^2\}$, always equal to or less than this number. For the case we introduce in subsection 4.2, $d = 6$ and there exists 6 constants in the first row of $K(u)$, neural networks are used to generated the other entries in $K(u)$. The rank of matrix C is less than or equal to $\min\{N_K, d * (d - 1)\}$,

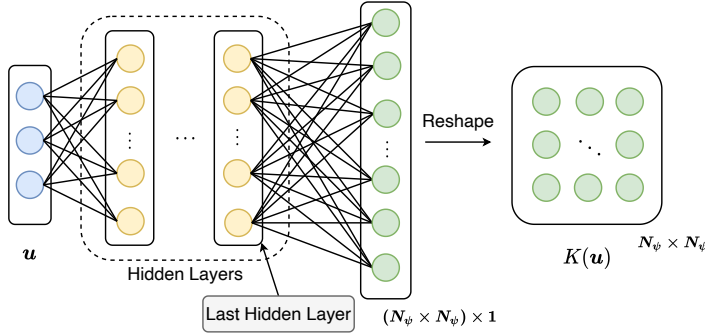


Fig. 9: The Neural Networks architecture of $K(u)$.

Appendix D. Analysis on Van der Pol Matheiu case with low non-linearity. In the case where the parameter $\mu = 0$, the PK-NN model does not perform as well as models M2 and M3. However, the structure of PK-NN can encompass the capabilities of both M2 and M3 models. To understand the reason why PK-NN is outperformed, its structure is set to include a “hardtanh” (originally “tanh” in the experiment before) activation function in the hidden layer, and it initially adopts the same weights and biases for the output layer as the successful model M2. The initial setup is slightly modified (perturbed) from this configuration and PK-NN is retrained. The outcomes reveal that the performance of PK-NN, which is indicated by a purple curve becomes similar to that of M2 with this precise initialization. Additionally, the blue curve shows the performance of PK-NN with the same “hardtanh” activation function but starting from a random initialization, highlighting that PK-NN struggles to learn effectively from scratch but can achieve good results with a suitable initialization. The results are shown in Figure 10. This finding suggests that the primary challenge with PK-NN is its trainability rather than its fundamental design.

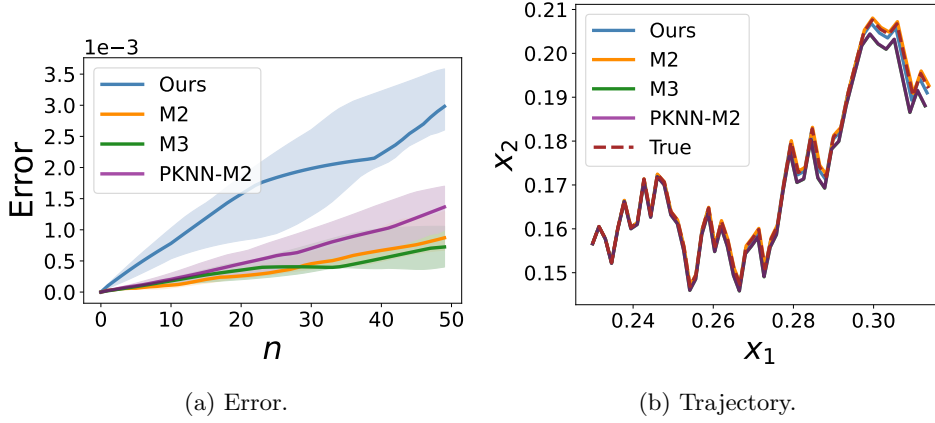
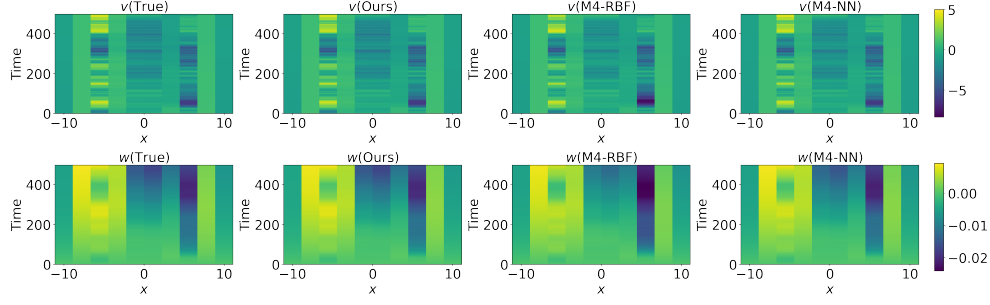
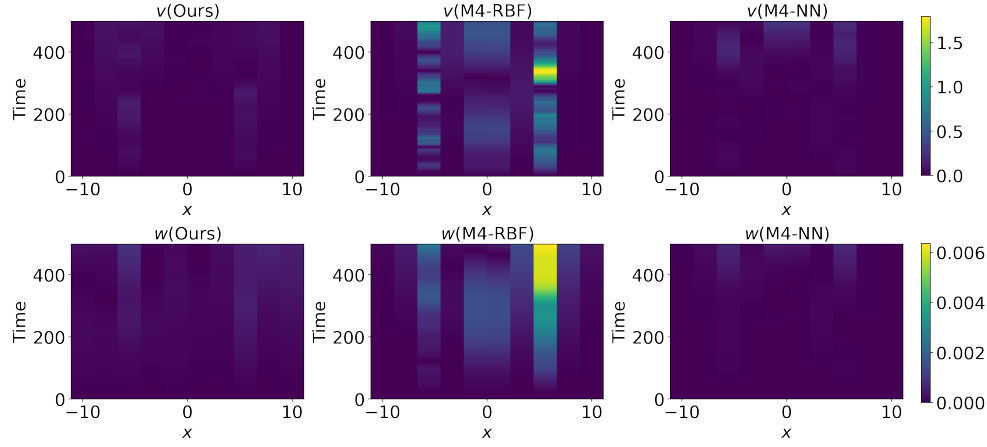


Fig. 10: The performance of PK-NN with perturbation on a precise initialization, which is the same as M2 setting, shown as PKNN-M2.

Appendix E. Trajectory results in original space for the FitzHugh-Nagumo system. Here are the results about trajectories on the original two-dimensional space of FitzHugh-Nagumo system and the difference between the prediction and the ground truth. The results in Figure 5 is about the case with $N_x = 10$ and $\dim \mathbf{u} = 1$. Figure 11 and Figure 12 show for different spatial discretisations ($N_x = 100$, $\dim \mathbf{u} = 1$) and control dimensions ($N_x = 10$, $\dim \mathbf{u} = 3$). We can see the performance among PK-NN, M4-RBF and M4-NN directly. Our PK-NN outperforms the other two models in all cases.

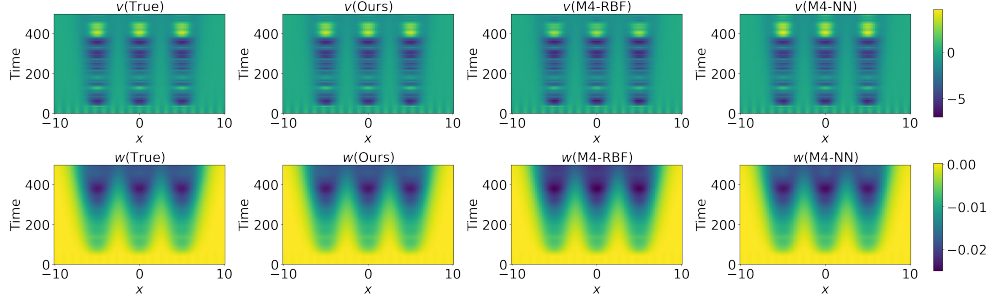


(a) Trajectory.

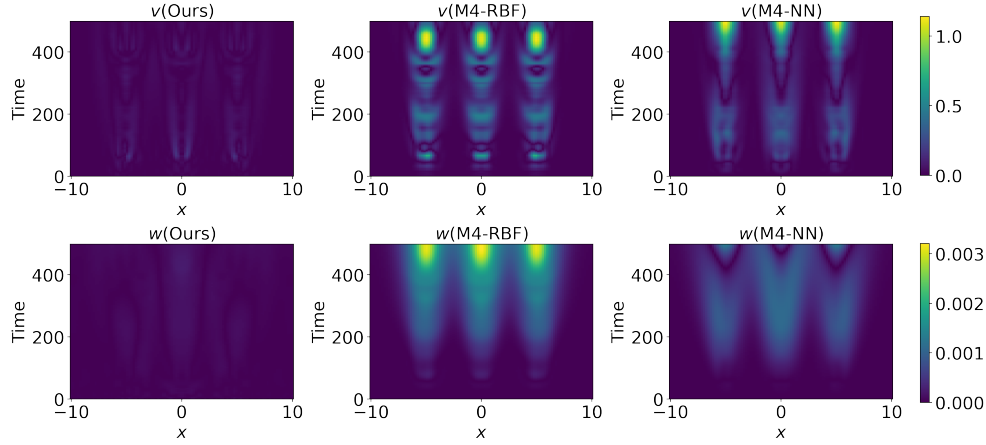


(b) Difference.

Fig. 11: (a): Predictions by PK-NN, M4-RBF and M4-NN on FHN system with $N_\psi = 10$ and $\dim \mathbf{u} = 3$. (b): The absolute value of the difference between the forecasted outcomes and the ground truth.



(a) Trajectory.



(b) Difference.

Fig. 12: (a): Predictions by PK-NN, M4-RBF and M4-NN on FHN system with $N_\psi = 100$ and $\dim \mathbf{u} = 1$. (b): The absolute value of the difference between the forecasted outcomes and the ground truth.

Appendix F. Latent space evolution of the Korteweg-De Vries system.

We show the evolution on the latent Koopman space of PK-NN for the Korteweg-De Vries (KdV) system in Figure 14. The solution of KdV equation is generated by a sequence of control u_i 's. Controls are applied on the trained PK-NN, the solution is evolved by it as shown in Figure 13 and the predicted mass and momentum are shown at the bottom. The evolution of entries in $K(\mathbf{u})$ as \mathbf{u} changes is shown in Figure 15. The evolution of “mass” mainly depends on the constant term, “mass” itself and $NN2$, multiplied by the second row’s first, second and fifth element in $K(\mathbf{u})$. The multiplications of the entry in $K(\mathbf{u})$ and its corresponding element in the dictionary are over 10^{-4} for these three components, larger than for others. The evolution of “momentum” mainly depends on the components of the latent space except “mass” since only the multiplication of the second element of the third row of $K(\mathbf{u})$ and “mass” is around 10^{-6} . We also find that the evolution of $NN1$ and $NN2$ have a linear relationship in Figure 16, which inspires us to figure out how to reduce the redundant ones in the dictionary.

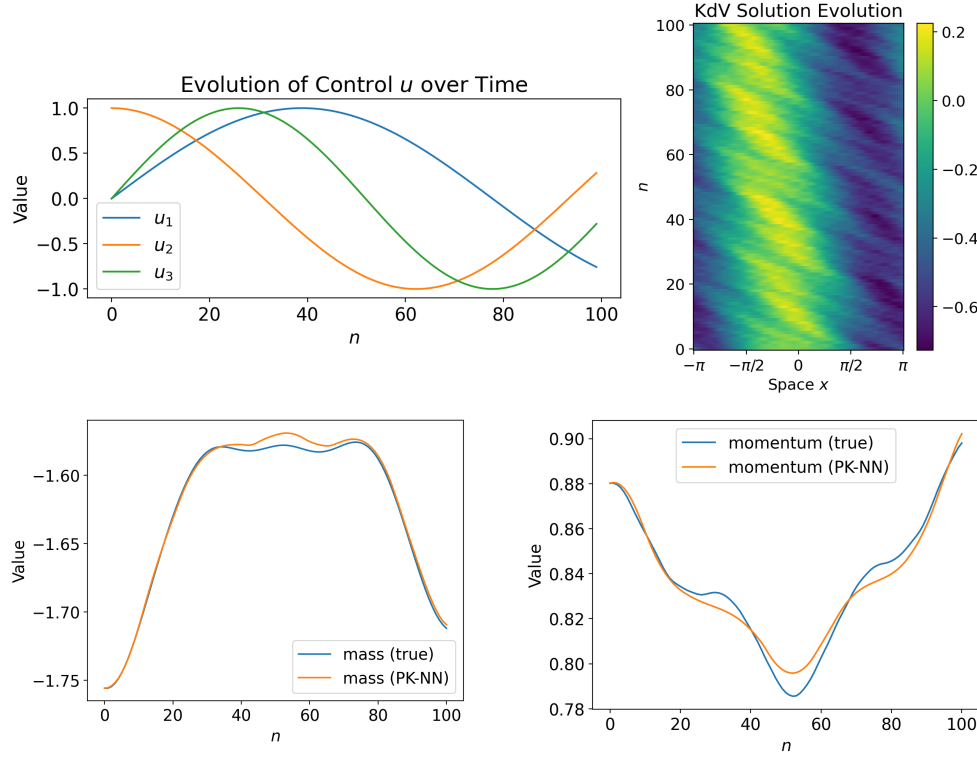


Fig. 13: The solution of KdV equation is generated by a sequence of control u_i 's. Controls are applied on the trained PK-NN model and the latent space is evolved by the Koopman operator. The predicted mass and momentum are shown at the bottom.

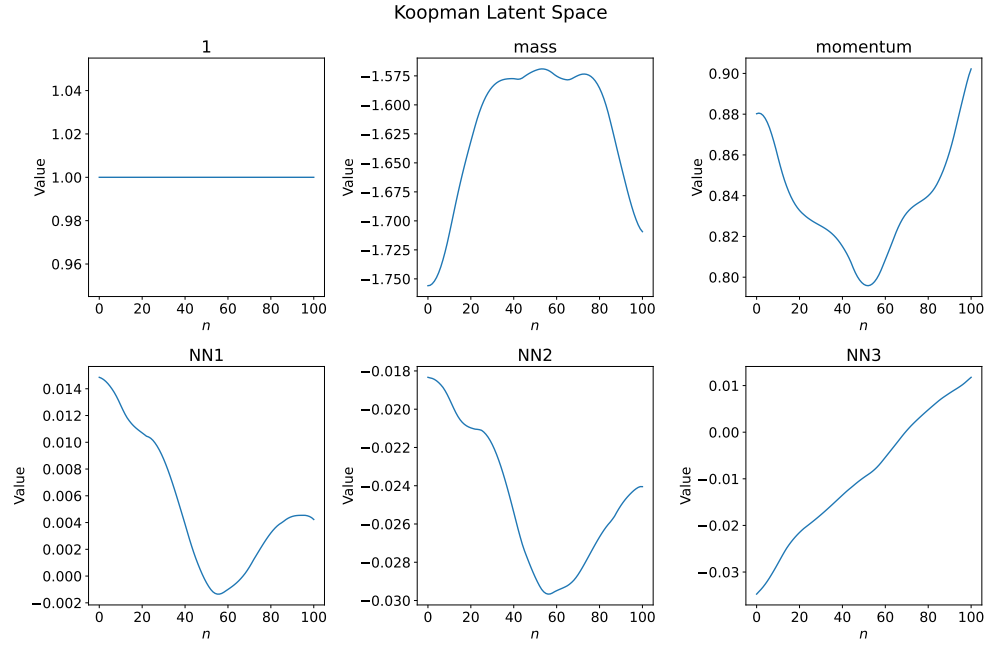


Fig. 14: Evolution on the latent space for the Korteweg-De Vries System. The “mass” and “momentum” are target observables. $NN_i, i = 1, 2, 3$ are trainable components in the dictionary.

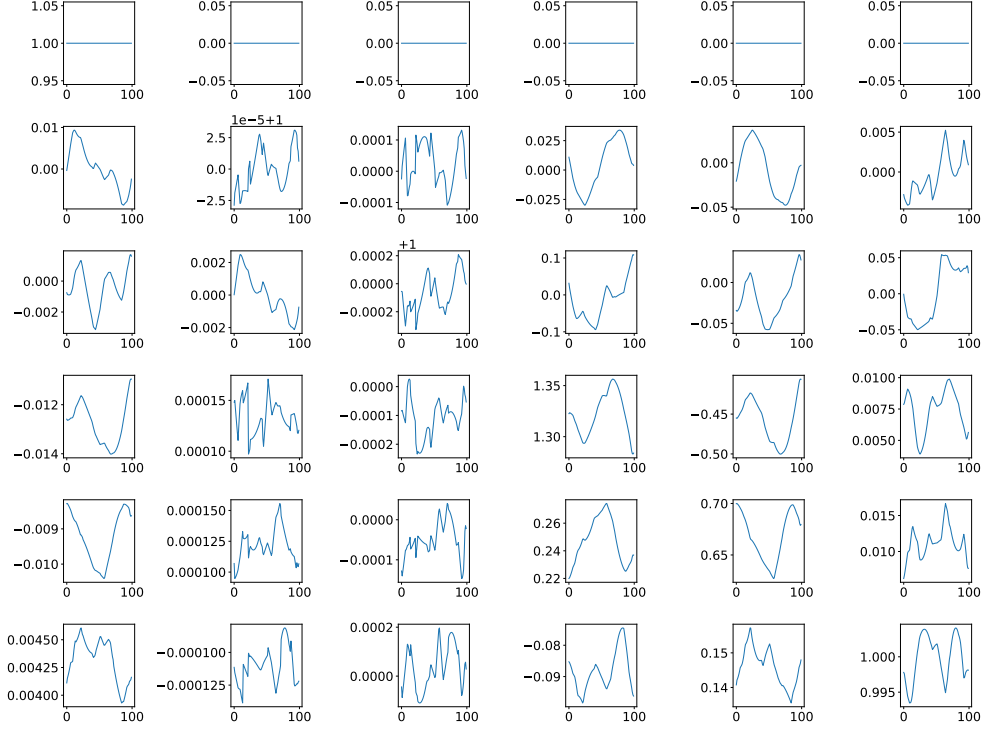
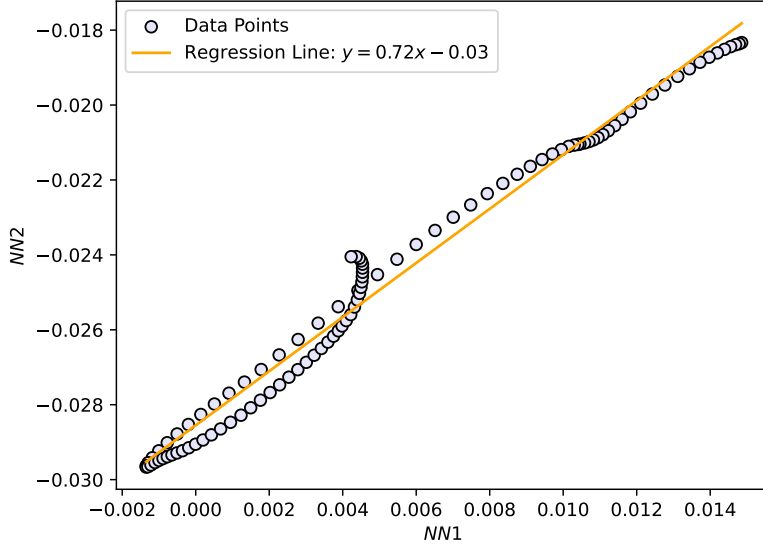


Fig. 15: The evolution of entries in $K(\mathbf{u})$ as \mathbf{u} changes. The first row is set as $(1, 0, \dots, 0)^T$ and others are trainable. In this matrix, the diagonal elements corresponding to the second and third rows are optimized to approximate values close to one, a configuration that aligns well with predictions related to mass and momentum. The forecast for the subsequent step is primarily influenced by the current state, along with some other non-linear terms about \mathbf{u} and \mathbf{x} .

Fig. 16: The relationship between $NN1$ and $NN2$.

Appendix G. Prediction results for mass and momentum of Korteweg-De Vries system. We compare the predictions of mass and momentum for KdV system by PK-NN, linear (M2) and bi-linear (M3) in Figure 17. Using Algorithm 3.2 and the metric defined in (4.1), we compute the relative error based on five trajectories with different initial conditions and plot the corresponding error bars. Observing over 10 time steps, which matches the horizon τ in MPC, we find that PK-NN outperforms the other two models in both mass and momentum predictions. This demonstrates that PK-NN can predict the observables m_{i+1} in (4.10) more accurately, laying a strong foundation for addressing the control problems.

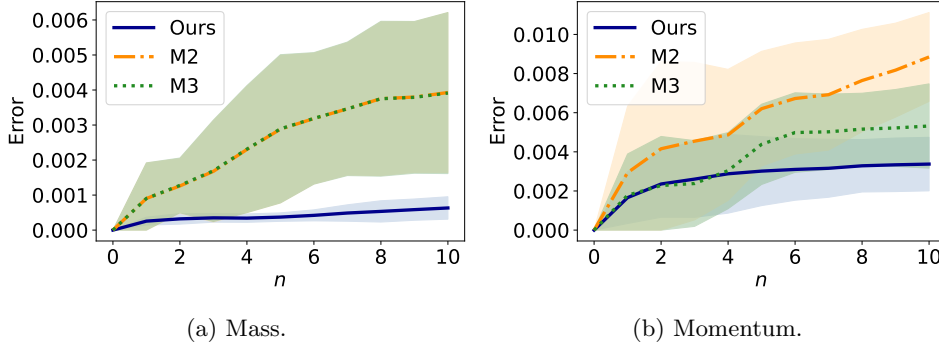


Fig. 17: The prediction results for mass and momentum of KdV system by PK-NN, M2 and M3.

Appendix H. PK-NN hyperparameter selection via cross-validation.

In this section, we provide a detailed explanation of the hyperparameter selection

process for PK-NN. We employ cross-validation with grid search to assess the model’s performance across various hyperparameters and train models with the same training strategies, including rules for learning rate decay and saving checkpoint criteria. We have a comprehensive explanation of how we choose the hyperparameters. The evaluation focuses on different aspects for each system:

- To investigate the impact of dictionary size on model performance, we employ the parametric Duffing system as a case study. It is generally presumed that a sufficiently large dictionary is crucial for accurately capturing the dynamics of the system. Nonetheless, training becomes increasingly challenging with larger dictionary sizes. We assessed the model’s performance using various dictionary sizes 5, 10, 15, 20, and 25, and observe improvements in performance with each increment in dictionary size. Consequently, we selected a dictionary size of 25 for our experimental framework. The results are shown in [Table 3](#).
- To explore the effect of the number of hidden nodes in $K(\mathbf{u})$ on performance, we choose the Van der Pol Mathieu system as an illustrative example, which has strong non-linearity on \mathbf{u} and \mathbf{x} . We evaluate the performance of the model across various configurations of hidden nodes [32], [64], [128], [32, 32], [64, 64] and [128, 128]. We find that two hidden layers do not enhance performance in comparison to a single-layer setup. Consequently, we choose single layer with 128 hidden nodes in our experiments, as this configuration achieves an error magnitude satisfactorily low, around 10^{-9} . The cross-validation results are shown in [Table 4](#).
- To show the effectiveness in situations involving high-dimensional state spaces, we assess the influence of varying numbers of hidden nodes in the dictionary neural network on the FitzHugh-Nagumo system. Our analysis reveals that the performance of models exhibits sensitivity to changes in the number of hidden nodes, with configurations tested including [32], [64], [128], [32, 32], [64, 64], and [128, 128]. Based on our findings, we select a configuration with two hidden layers, each comprising 128 nodes. This configuration leads to a significant improvement in error, around 10^{-7} , detailed in [Table 5](#).

By evaluating the effect of hyperparameters on neural networks, it often emerges that opting for one or two hidden layers, each with 128 nodes, within the dictionary neural network presents an optimal strategy. Similarly, for the $K(\mathbf{u})$ architecture, selecting one or two hidden layers with a width of 128 tends to be a suitable choice. For the activation functions in $K(\mathbf{u})$ hidden layers, “tanh” works more effectively than “ReLU” if the depth is one or two. Regarding the size of the dictionary, our recommendation leans towards choosing a larger size. However, it’s important to consider that a larger dictionary results in a more complex $K(\mathbf{u})$ matrix, which leads to higher computational demands and greater challenges in training. Therefore, the decision on hyperparameters should be balanced with the performance and the computational capabilities available.

$N_\psi \backslash \text{Task}$	$\nu_1 = 1000, \nu_2 = 10$	$\nu_1 = 500, \nu_2 = 20$	$\nu_1 = 100, \nu_2 = 100$
5	1.25×10^{-4}	3.83×10^{-5}	4.74×10^{-4}
10	6.46×10^{-5}	1.09×10^{-5}	3.48×10^{-4}
15	4.48×10^{-5}	8.11×10^{-6}	1.29×10^{-4}
20	2.10×10^{-5}	4.35×10^{-6}	1.12×10^{-4}
25	1.42×10^{-5}	4.68×10^{-6}	1.01×10^{-4}

Table 3: Cross-validation results for the case of parametric duffing system.

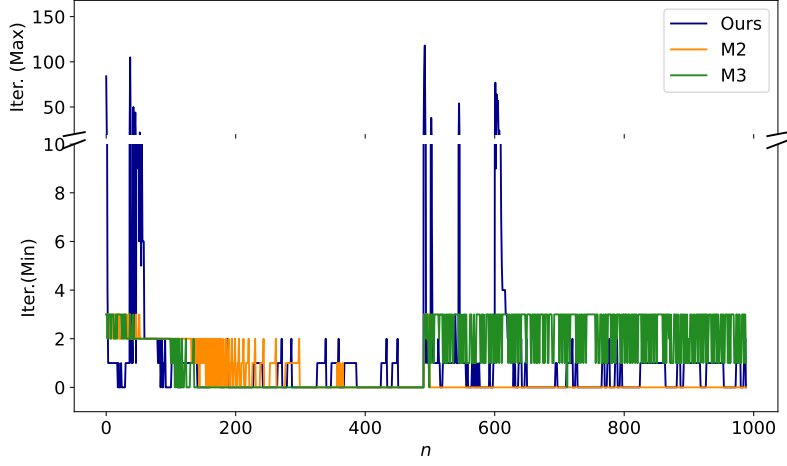
$K(\mathbf{u}) \backslash \text{Task}$	$\mu = 0$	$\mu = 1$	$\mu = 2$	$\mu = 3$	$\mu = 4$
[32]	1.08×10^{-8}	1.34×10^{-8}	1.27×10^{-8}	1.76×10^{-8}	2.26×10^{-8}
[64]	7.12×10^{-9}	8.12×10^{-9}	9.28×10^{-9}	1.09×10^{-8}	1.98×10^{-8}
[128]	6.23×10^{-9}	7.02×10^{-9}	8.31×10^{-9}	1.47×10^{-8}	1.15×10^{-8}
[32, 32]	6.05×10^{-9}	7.91×10^{-9}	8.43×10^{-9}	1.49×10^{-8}	2.71×10^{-8}
[64, 64]	6.75×10^{-9}	6.48×10^{-9}	7.07×10^{-9}	1.36×10^{-8}	2.26×10^{-8}
[128, 128]	8.28×10^{-9}	8.80×10^{-9}	8.29×10^{-9}	1.36×10^{-8}	2.01×10^{-8}

Table 4: Cross-validation results for the case of Van der Pol Matheiu system.

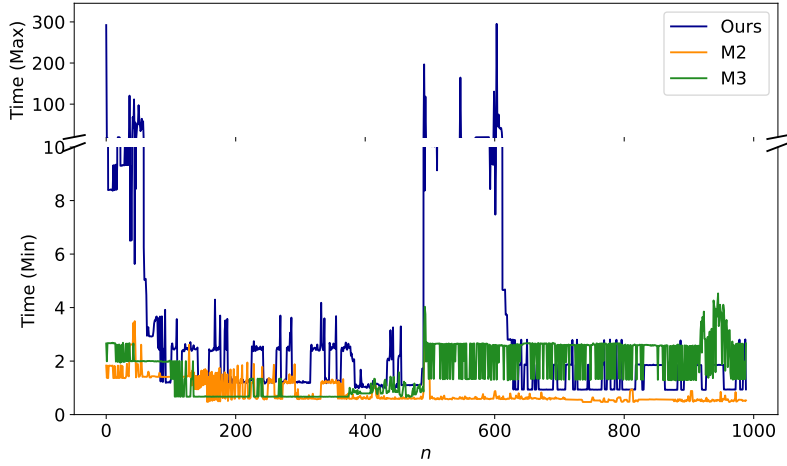
$\Psi(\mathbf{x}) \mid$	[32]	[64]	[128]	[32, 32]	[64, 64]	[128, 128]
Loss	1.82×10^{-6}	6.66×10^{-7}	2.47×10^{-7}	7.77×10^{-7}	3.41×10^{-7}	1.45×10^{-7}

Table 5: Cross-validation results for the case of FitzHugh-Nagumo system ($N_x = 100, \dim \mathbf{u} = 1$).

Appendix I. Comparison about the computational cost of optimal control problems. We examine the computational costs associated with solving optimal control problems for the Korteweg-De Vries (KdV) system. We consider the tracking momentum problem, with a focus on a system influenced by non-linear (sin) forcing, setting $\lambda = 0.005$ as an example. A key strategy in our optimization process is to initialize the parameters to be optimized using the outcomes from the previous step. This iterative initialization significantly decreases the optimization time, particularly when consecutive control values are closely related. We show both the optimization time and the iteration count for each step, as detailed in Figure 18. Our findings indicate that the computational demands of the PK-NN model are comparably higher than those of other models. The iteration times for models M2 (linear) and M3 (bilinear) are around 1 second, whereas for the PK-NN model, they vary between 1 and 8 seconds. The optimization averages 5.82 seconds for PK-NN, 0.83 seconds for M2, and 1.69 seconds for M3. Consequently, with the same optimizer in use, the PK-NN model requires 3 to 7 times more time to complete each iteration compared to the other two methods.



(a) The number of iterations for each optimization.



(b) Cost of time for each optimization.

Fig. 18: Computational cost of the optimization in KdV tracking problem by PK-NN, M2 and M3.